University of Kentucky
UKnowledge

KWRRI Research Reports   Kentucky Water Resources Research Institute

8-1984

Finite Element Simulation of Saturated-Unsaturated Subsurface Flow

George E. Blandford
University of Kentucky

Right click to open a feedback form in a new tab to let us know how this document benefits you.

Follow this and additional works at: https://uknowledge.uky.edu/kwrri_reports

Part of the Hydrology Commons, and the Water Resource Management Commons

FINITE ELEMENT SIMULATION OF

SATURATED-UNSATURATED

SUBSURFACE FLOW

By

George E. Blandford

Principal Investigator

Project Number: A-091-KY (Completion Report)

Agreement Number: G-844-03   (FY 1983)

Period of Project: July 1983 – August 1984

Water Resources Research Institute
University of Kentucky
Lexington, Kentucky

August 1984

DISCLAIMER

Contents of this publication do not necessarily reflect the views and policies of the U.S. Department of the Interior, nor does mention of trade names or commercial products constitute their endorsement by the U.S. government.

ABSTRACT

A two-dimensional transient model for flow through saturated-unsaturated porous media is developed. The model numerically solves the pressure head dependent or moisture content dependent form of Richard's equation. The model code uses isoparametric quadratic triangular and/or quadrilateral finite elements for the geometric representation and for the weak Galerkin spacial integrations. An implicit, unconditionally stable single-step numerical time integration scheme with an oscilliatory noise reduction option is utilized for the temporal discretization. The highly efficient symmetric skyline (profile) solution scheme is used to solve the resulting simultaneous equations. The nonlinear subsurface flow parameters are approximated using cubic spline interpolation. The element material properties can be independently defined thus permitting the modelling of layered geologic formations. Derivative smoothing is presented for the post-calculation of Darcian velocities. Currently, the program is limited to time varying specification of pressure head or moisture content and fluxes. Several sample problems are presented illustrating the accuracy and validity of the developed model.

DESCRIPTORS: Mathematical Models; Model Studies; Saturated Flow;
              Unsaturated Flow; Storm Seepage; Finite Element Method

IDENTIFIERS: Subsurface Flow; Two-dimensional Transient Model

ACKNOWLEDGEMENTS

TABLE OF CONTENTS

LIST OF FIGURES

NOTATION

General

$\overline{n}$ — unit inward normal vector

t — time

x,y — cartesian coordinates

$\overline{X}$ — cartesian coordinate vector

∇ — gradient operator

Differential Equations

e — soil medium dilation

g — acceleration of gravity

h — pressure head

h_o — initial pressure head

$\overline{h}$ — prescribed pressure head

h_L — minimum soil surface pressure head

H — hydraulic head

q — prescribed flux

$\overline{V}_s$ — solid velocity vector

$\overline{V}_{fs}$ — velocity vector of the fluid with respect to the solid; Darcian velocity vector

V_x, V_y — cartesian components of the Darcian velocity vector

V_p — prescribed potential flux

Z — elevation head

Θ — moisture content

Θ_o — initial moisture content

$\overline{\Theta}$	–	prescribed moisture content
Θ_R	–	irreducible moisture content
Θ_s	–	saturated moisture content
Ω	–	domain
Γ	–	boundary of Ω'
Γ_1	–	pressure head/moisture content boundary
Γ_2	–	flux boundary

Material coefficients

D^r	–	relative soil moisture diffusivity
F	–	generalized storage coefficient
$\overline{\overline{K}}$	–	hydraulic conductivity tensor
$\overline{\overline{K}}^s$	–	saturated hydraulic conductivity tensor
K^s_{xx}, K^s_{xy} K^s_{yx}, K^s_{yy}	–	components of the saturated hydraulic conductivity tensor
K^r	–	relative hydraulic conductivity
n	–	porosity
S	–	degree of saturation
α	–	coefficient of consolidation
α'	–	modified coefficient of consolidation
ρ	–	fluid density
λ_s, μ_s	–	Lame' constants for the soil medium

Finite Element

$A(\ ),\ C(\ )$	–	lower order domain differential operators
$B(\ )$	–	differential operator evaluated along the boundary
$D_f(\ )$	–	domain differential equation
$I(\ )$	–	integrand

L_1, L_2, L_3	–	triangular element area coordinates
L_{1i}, L_{2i}	–	i-th quadrature point area coordinates
n	–	time step
n_e	–	number of element shape functions
n_g	–	number Gauss quadrature points
N_e	–	number of finite elements
N_i^e	–	node i shape function for element e
$\overline{N_i^e}$	–	evaluation of N_i^e along the element boundary
N_t	–	number of time steps
R	–	residual
$\tilde{V}$	–	smoothed Darcian velocity vector
w_i	–	i-th Gauss quadrature weighting coefficient
W	–	weighting function
ξ, η	–	nondimensionalized local coordinates for the quadrilateral element
ξ_i, η_i	–	i-th Gauss quadrature point coordinates
ε	–	prescribed convergence tolerance
δ	–	time weighting coefficient
Ω^e	–	element subdomain
Γ^e	–	element boundary

Matrix

[ ]	–	signifies row vector
{ }	–	signifies column vector
[ ]	–	signifies matrix
$\left[D(\Theta)\right]$	–	moisture content dependent diffusivity matrix
$\left[D^e(\Theta)\right]$	–	element level diffusivity matrix
[J]	–	Jacobian matrix

$[J]^{-1}$ — inverse Jacobian matrix

$|J|$ — Jacobian determinant

J_Γ — boundary Jacobian

$[K(h)]$ — pressure head dependent conductivity matrix

$[K^e(h)]$ — element level conductivity matrix

$[N]$ — vector of element shape functions

$[\tilde{N}]$ — vector of element shape functions for spacial interpolation of the material data and Darcian velocity smoothing calculations

$\{Q(h)\}$ — pressure head dependent flow domain load vector

$\{Q(\Theta)\}$ — moisture content dependent flow domain load vector

$\{Q_p\}$ — point source/sink load vector

$\{r_q\}$ — quadrilateral element velocity smoothing right hand side vector

$\{r_t\}$ — triangular element velocity smoothing right hand side vector

$[S]$ — linear storage matrixfor moisture content analysis

$[S^e]$ — element level linear storage matrix

$[S(h)]$ — pressure head dependent storage matrix

$[S^e(h)]$ — element level storage matrix

$[S_q^e]$ — quadrilateral element velocity smoothing matrix

$[S_t^e]$ — triangular element velocity smoothing matrix

involved in the preparation of environmental impact studies, water management planners and agriculturists. This group of beneficiaries includes county health departments, state water quality agencies, U.S. EPA, consulting engineers and other researchers. Researchers and consulting engineers will especially benefit from this research since the program can be used separately or in combination for analyzing aquifer performance subjected to recharge, evaporation and/or transpiration, seepage through earth dams and for irrigation and drainage problems.

I.2 BACKGROUND

Early work in the numerical analysis of two-dimensional saturated-unsaturated porous media flow was performed using the finite difference method, e.g., Rubin (1968) and Freeze (1971, 1972 (a) and (b)). Due to the limitations of the finite difference method, researchers began using the more powerful and flexible finite element method.

Neuman (1973) was one of the first investigators to use the finite element method for the analysis of saturted-unsaturated porous media flow. Neuman used a Galerkin spatial finite element formulation with linear triangular elements and an under relaxation scheme in time for the analysis of saturated-unsaturated seepage flow. He outlined the procedure for combining four triangular elements to form a single quadrilateral element. Neuman also correctly pointed out that the triangular and quadrilateral elements for two-dimensional analysis can be extended for the analysis of axisymmetric subsurface flow problems. Neuman et al. (1975) extended the finite element formulation of Neuman (1973) to include water uptake by roots. Feedes et al. (1975) compared the predicted finite element solution of Neuman et al. (1975) with field measured data on one-dimensional and two-dimensional problems. A good correlation was obtained between the predicted finite element results and

2

CHAPTER I

INTRODUCTION

I.1 SIGNIFICANCE OF WORK

The modelling of saturated-unsaturated groundwater zones has received increased activity in recent years. The reason for this activity is that the Environmental Protection Agency, the Kentucky Water Resources Research Institute and other agencies have recognized the potential hazards of contaminant infiltration into groundwater supplies from uncontrolled toxic waste dumping, municipal and industrial wastewaters, sludge from water and wastewater treatment plants, and solid wastes, from a broad range of activities, which are discharged onto farmlands, surface mining reclamation areas and to other open areas. Hence, a prediction of the movement of infiltrated contaminants in groundwater supplies is necessary to prevent long-range disasters.

Groundwater is also one of the components of the hydrologic cycle. Hence, its quantity and movement are of critical importance to hydrologists and agronomists.

The long term purpose of the computer model developed in this report is to provide a scientific analysis for subsurface flow and contaminant transport in porous media. Two computer programs can be used, based on the physics of two-dimensional subsurface flow and contaminant transport in saturated-unsaturated porous media. The moisture contents and Darcian velocities from a subsurface flow analysis can be used as input to the contaminant transport program for the prediction of non-conservative contaminant migration.

The results of this research can be of great importance to people

1

the field observations.

Reeves and Duguid (1975) used a spatial Galerkin finite element formulation with bilinear quadrilateral elements and a weighted difference scheme in time for their analysis of two-dimensional saturated-unsaturated porous media flow. Their computer program was written to include pressure-dependent boundary conditions at the ground surface. Thus, infiltration or seepage could be simulated. Reeves and Duguid found that their finite element program reduced computer running time by half when compared to the finite difference program by Freeze (1972 (a) and (b)).

The representation of the nonlinear material properties has also received a considerable amount of attention by researchers in this area. Field data is not easily available and if available is not presented in a very convenient manner. The basic relationships are highly nonlinear and are tabulated at irregular intervals. A convenient but inaccurate method involves the linear interpolation within each interval. Campbell (1974) proposed a simple method of determining the relative hydraulic conductivity as a function of the degree of saturation from the soil water retention curve. This method assumes and is valid only if there is an exponential relationship between the potential and moisture content, i.e., water retention function plots as a straight line on a log - log scale, Gardner et al. (1970). If these conditions are sastisfied Campbell's equation can be used to find an analytic expression relating hydrulic conductivity and potential. Since this formulation breaks down near saturation, Clapp and Hornberger (1978) used a short parabolic section in this region to represent gradual air entry. The restricted nature of the exponential-parabolic representation makes it unsuitable for a general treatment of nonlinear material properties in groundwater flow.

The investigation presented in this report considers the development of a two-dimensional finite element model for flow through saturated-unsaturated porous media. The model is based on the pressure head or moisture content form of Richard's equation. Six node triangular and/or eight node quadrilateral isoparametric elements are utilized for geometric representation and in the weak Galerkin spacial integrations. These elements represent a quadratic spacial modeling. Consequently, they are generally more accurate than the linear finite element models discussed in the previous section. The transient behavior of Richard's equation is approximated using an implicit (unconditionally stable) single-step linear time interpolation scheme. An oscilliatory noise reduction technique is also presented for the implicit time algorithms which are oscillation prone (e.g., the Crank-Nicolson scheme).

The analytical representation using Campbell's (1974) and Clapp & Hornberger's (1978) expressions is very restricted in scope and cannot be used generally. Consequently, cubic spline interpolation, using packaged subroutines from IMSL library (1982), was incorporated into the computer program for representation of the nonlinear material properties. Nonlinear material properties are input in a tabular form and a cubic spline interpolation, with first or second derivatives specified at the end points, is used to approximate the material parameters during the iterative process.

The direct iteration or successive substitution method is presented for iteratively solving the saturated-unsaturated subsurface flow equations. Nonlinear boundary conditions associated with seepage faces and/or infiltration/evaporation are discussed. The skyline or profile simultaneous equation solution process is utilized in the model to minimize computer time and storage in generating the time dependent iterative solutions. An integral

least squares derivative smoothing procedure is used to obtain the element node Darcian velocities.

Finally, several numerical examples are presented to demonstrate the validity and accuracy of the developed model. The examples include linear and nonlinear steady state simulations as well as linear and nonlinear transient simulations.

CHAPTER II

GOVERNING EQUATIONS

The mathematical model used in this study is Richard's equation, valid
for both saturated and unsaturated subsurface flow. As with any mathematical
model, Richard's equation is based on some simplifying assumptions. In
particular, the assumptions utilized in this investigation are:

1. The fluid medium is continuous.

2. The soil matrix is continuous.

3. The fluid is in motion.

4. The soil medium undergoes consolidation.

5. The fluid is incompressible.

6. The air phase is continuous and is at atmospheric pressure.

7. Flow is laminar and Darcy's law is valid.

II.1 FORMULATION OF THE PRESSURE HEAD FLOW EQUATION

The development of Richard's equation which includes the seven
aforementioned assumptions requires the utilization of (Reeves amd Duguid,
1975) (1) fluid continuity, (2) solid continuity, (3) fluid motion, and (4)
medium consolidation. These four equations will be presented in the following
paragraphs and then combined to form a single governing equation, i.e.,
Richard's equation.

The fluid continuity is expressed as (Cooper, 1966)

$$\frac{\partial (S \rho n)}{\partial t} + \nabla \cdot \rho n S \overline{V}_s + \nabla \cdot \rho \overline{V}_{fs} = 0 \qquad (II.1)$$

where n is the porosity, S is the degree of saturation, ρ is the density of water, $\overline{V}_s$ is the velocity vector of the solid, $\overline{V}_{fs}$ is the velocity vector of the fluid relative to the solid and ∇ is the two-dimensional gradient operator. The term velocity refers to Darcian velocity or Darcian flux of the fluid relative to the solid.

The granular skeleton of the medium is considered compressible, however, the grains which make up the skeleton are considered incompressible. The continuity equation for the incompressible grains is

$$\frac{\partial(1-n)}{\partial t} + \nabla \cdot (1-n)\overline{V}_s = 0 \qquad (II.2)$$

where (1-n) represents the volume concentration of the solids.

The equation of motion for the fluid is Darcy's law for an anisotropic medium, i.e.,

$$\overline{V}_{fs} = -\overline{\overline{K}} \cdot \nabla H \qquad (II.3)$$

where H is the hydraulic head and $\overline{\overline{K}}$ is the hydraulic conductivity tensor. Equation II.3 can be rewritten in terms of the pressure head, h, and the elevation head, Z, as

$$\overline{V}_{fs} = -\overline{\overline{K}} \cdot (\nabla h + \nabla Z) \qquad (II.4)$$

The anisotrophy in the hydraulic conductivity is the result of assuming that the soil medium is composed of orthotropic layers. Further, the principal axes of orthotropy (local) are assumed to differ from the reference coordinate system (global). Figure II.1(a) shows a typical soil layer and its principal axes of orthotropy. Figure II.1(b) gives the resulting anisotropic tensor via a double coordinate transformation on the principal axis

conductivity coefficients.

The consolidation of the medium is based on Terzaghi's (1925) one-dimensional consolidation theory. This limitation to a one-dimensional consolidation theory is reasonable due to the large lateral extent of the soil masses being investigated. The use of Terzaghi's one-dimensional consolidation theory leads to (Reeves and Duguid, 1975)

$$\frac{\partial e}{\partial t} = \alpha \frac{\partial p}{\partial t} \tag{II.5}$$

where e is the soil medium dilatation, α is the coeficient of consolidation; $\alpha = \frac{1}{\lambda_s + 2\mu_s}$, and λ_s, μ_s are Lame's constants for the soil medium. Since a one-dimensional consolidation approximation has been utilized, only the vertical displacement, $\overline{u}$, is nonzero which leads to the following definitions

$$e = \nabla \cdot \overline{u}$$

$$\overline{V}_s = \frac{\partial \overline{u}}{\partial t} \tag{II.6}$$

Using the relationships given by Eqs. II.5, II.6 and $p = \rho g h$ leads to

$$\nabla \cdot \overline{V}_s = \frac{\partial e}{\partial t}$$

$$= \alpha \frac{dp}{dh} \frac{\partial h}{\partial t}$$

$$= \alpha' \frac{\partial h}{\partial t} \tag{II.7}$$

where

$$\alpha' = \alpha \rho g$$

is the modified coefficient of consolidation for the medium.

Now, expanding Eq. II.1 gives

$$\frac{\partial(\rho n S)}{\partial t} + \nabla \cdot \rho n S \overline{V}_s + \nabla \cdot \rho \overline{V}_{fs}$$

$$= \rho n \frac{\partial S}{\partial t} + \rho S \frac{\partial n}{\partial t} + \rho S \nabla \cdot (n \overline{V}_s)$$

$$+ \nabla \cdot \rho \overline{V}_{fs} + n \overline{V}_s \cdot \nabla(\rho S) = 0 \qquad \text{(II.8)}$$

where the last term in Eq. II.8 may be neglected as a higher-order effect
(Reeves and Duguid, 1975). Substituting the following relationships

$$\theta = nS$$

- moisture content

$$n \frac{\partial S}{\partial t} = n \frac{dS}{dh} \frac{\partial h}{\partial t}$$

$$= \frac{d\theta}{dh} \frac{\partial h}{\partial t}$$

$\frac{d\theta}{dh}$ - specific moisture capacity

$$\frac{\partial n}{\partial t} = \nabla \cdot (1-n) \overline{V}_s$$

$$= \nabla \cdot \overline{V}_s - \nabla \cdot n \overline{V}_s$$

$$= \alpha \frac{\partial h}{\partial t} - \nabla \cdot n \overline{V}_s$$

(see Eqs. II.2 and II.7)

and Eq. II.4 into Eq. II.10 results in

$$\left[\frac{\theta}{n} \alpha' + \frac{d\theta}{dh} \right] \frac{\partial h}{\partial t} = \nabla \cdot \left[\overline{\overline{K}}(\nabla h + \nabla Z) \right] \qquad \text{(II.11)}$$

Introducing

$$F(h) = \frac{\theta(h)}{n} \alpha' + \frac{d\theta(h)}{dh}$$

- a generalized storage coefficient

$$\overline{\overline{K}}(h) = K^r(h) \overline{\overline{K}}^s$$

9

where $K^r(h)$ is the relative hydraulic conductivity ($0 < K^r(h) \le 1$; $K^r(h) = 1$ in the saturated zone) and $\overline{\overline{K}}^s$ is the saturated hydraulic conductivity tensor (see Fig. 1) into Eq. II.12 results the following quasilinear partial differential equation

$$F(h) \, \frac{\partial h}{\partial t} + \nabla \cdot \left[K^r(h)\overline{\overline{K}}^s(\nabla h + \nabla Z) \right] = 0 \qquad (II.12)$$

Equation II.12 reduces to the linear elastic storage equation if the aquifer is saturated. For unsaturated flow, Eq. II.12 is a nonlinear equation known as Richard's equation. Thus, Eq. II.12 is valid for both saturated and unsaturated subsurface flow.

II.2 FORMULATION OF THE MOISTURE CONTENT FLOW EQUATION

The development of the governing equation in the previous section (Eq. II.12) was based on the pressure head being the dependent variable. Equation II.12 is extensively utilized when simultaneously analyzing saturated and unsaturated subsurface flow. However, when the main interest is the unsaturated or partially saturated zone soil physicists have typically used a moisture content based formulation. The usual procedure in a moisture content based flow formulation is to neglect soil consolidation which transforms Eq. II.12 into

$$\frac{d\theta}{dh} \frac{\partial h}{\partial t} = \nabla \cdot \left[K^r(h)\overline{\overline{K}}^s(\nabla h + \nabla Z) \right] \qquad (II.13)$$

Substituting

$$\frac{\partial h}{\partial t} = \frac{dh}{d\theta} \frac{\partial \theta}{\partial t}$$

$$\nabla h = \frac{dh}{d\theta} \nabla \theta$$

results in

$$\frac{\partial \theta}{\partial t} = \nabla \cdot [K^r(\theta)\overline{\overline{K}}^s(\frac{dh}{d\theta} \nabla h + \nabla Z)]$$

$$= \nabla \cdot [K^r(\theta)\frac{dh}{d\theta} \overline{\overline{K}}^s \nabla h + K^r(\theta)\overline{\overline{K}}^s \nabla Z]$$

$$= \nabla \cdot [D^r(\theta)\overline{\overline{K}}^s \nabla h + K^r(\theta)\overline{\overline{K}}^s \nabla Z] \qquad (II.14)$$

where $D^r(\theta) = K^r(\theta)\frac{dh}{d\theta}$ is the relative soil-mositure diffusivity.

There are two primary advantages associated with using the θ-based Eq. II.14. First, there is no nonlinear coefficient on the left hand side of Eq. II.14 (compare with Eq. II.13). Second, $D^r(\theta)$ and $K^r(\theta)$ are much less nonlinear, for soils of low saturation, than either F(h) or $K^r(h)$. This means that the moisture content variations are more gradual than the corresponding pressure head variations (Narasimhan, 1975). Thus, the θ-based equation is easier to solve than the corresponding h-based equation.

The diffusivity concept and θ-based equation possesses disadvantages as well. The concept of diffusivity must take on a different meaning in the pressure head range, air-entry value $\leq$ h $\leq$ 0, since desaturation cannot occur in this range, i.e., (dS/dh) = 0. Furthermore, if porosity is assumed constant then (dθ/dh) = 0 which means (dh/dθ) = ∞ and $D^r(\theta) \rightarrow \infty$. This anomaly can be overcome by taking into account the soil skeleton deformation at or near saturation (Narasimhan, 1975). In the air-entry value $\leq$ h $\leq$ 0 range, the relative diffusity $D^r(\theta) = K^r(\theta)\frac{dh}{d\theta}$ should represent $K^r(\theta)\frac{dh}{dn}$ where n is the porsity. Thus, in this range of pressure head values the relative diffusivity becomes identical with the coefficient of consolidation, α (for proof, see Narasimhan, 1975, p. 59).

Another disadvantage of the θ-based flow equation is that it is limited to a homogenous medium. The moisture content between two different soil layers is not continuous whereas the pressure head is continuous. However, for flow regions which are homogenous and at low saturations, the θ-based equation should be used.

II.3 INITIAL AND BOUNDARY CONDITIONS

The solution of the pressure head flow equation (Eq. II.12) or the moisture content flow equation (Eq. II.14) requires the specification of initial and boundary conditions. The initial conditions consist of specifying h or θ everywhere within the solution domain Ω at time t = 0, i.e.,

$$h(\overline{X},0) = h_0(\overline{X}) \tag{II.15a}$$

$$\Theta(\overline{X},0) = \Theta_0(\overline{X}) \tag{II.15b}$$

The boundary conditions consist of specifying either the pressure head/moisture content or normal flux everywhere along the boundary Γ for $t \geq$ 0. In particular, letting Γ_1 represent the prescribed pressure head/moisture content boundary and Γ_2 the normal flux boundary leads to the following boundary condition statements

$$h(\overline{X},t) = \overline{h}(\overline{X},t) \quad \text{on} \quad \Gamma_1 \tag{II.16a}$$

$$\Theta(\overline{X},t) = \overline{\Theta}(\overline{X},t) \quad \text{on} \quad \Gamma_1 \tag{II.16b}$$

$$[K^r \overline{\overline{K}}^s (\nabla h + \nabla Z)] \cdot \overline{n} = q \quad \text{on} \quad \Gamma_2 \tag{II.17a}$$

$$[D^r K^s \nabla \Theta + K^r K^s \nabla Z] \cdot \overline{n} = q \quad \text{on} \quad \Gamma_2 \tag{II.17b}$$

The values of $\overline{h}, \overline{\Theta}$ and q in Eqs. II.16 and II.17 are known functions of $\overline{X}$ and t, and n is the unit inward normal on Γ .

12
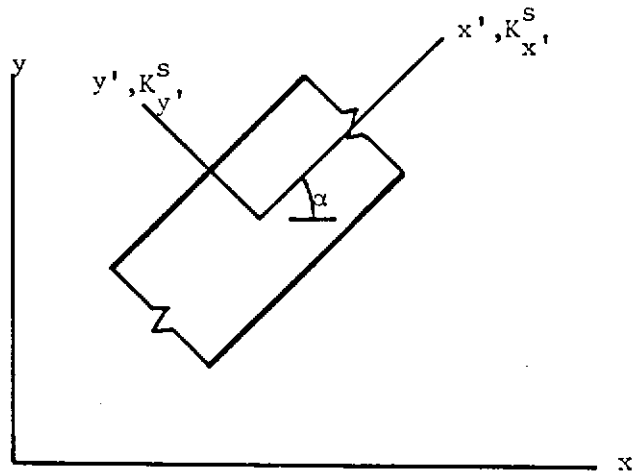
(a) Inclination of Soil Layer

$$K_{xx}^{S} = K_{x'}^{S} \cos^2\alpha + K_{y'}^{S}\sin^2\alpha$$

$$K_{xy}^{S} = K_{yx}^{S} = \tfrac{1}{2} \left(K_{x'}^{S} - K_{y'}^{S} \right) \sin2\alpha$$

$$K_{yy}^{S} = K_{x'}^{S}\sin^2\alpha + K_{y'}^{S} \cos^2\alpha$$

(b) Transformation of the Hydraulic Conductivities

FIG. II.1 - LAYERED ORTHOTROPIC POROUS MEDIA

13

CHAPTER III

NUMERICAL IMPLEMENTATION

The exact solution of the quasilinear partial differential equations (Eqs. II.12 and II.14) subject to the initial (Eq. II.15) and boundary (Eqs. II.16 and II.17) conditions is generally not possible. Consequently, recourse to approximate solution techniques is required. The purpose of this chapter is to describe the numerical approximation for the solution of two-dimensional saturated-unsaturated subsurface flow problems.

III.1 FINITE ELEMENT FORMULATION

The first step in the numerical approximation of the quasilinear partial differential equations is to choose the discretization strategy. This investigation is based on using a finite element discretization. Finite elements were chosen due to its ability to model irregular boundaries, mesh refinement/expansion capabilities and the ease in modelling complicated boundary conditions.

The finite element discretization/formulation involves three basic steps, i.e., (1) development of an integral relationship corresponding to the governing differential equation, (2) definition of the element geometric forms and (3) approximation of the unknown field variable. In this investigation, the weak Galerkin weighted residual method is used to construct the finite element integral equations. Isoparametric quadratic triangular and quadrilateral finite elements (Fig. III.1) are used to represent the flow

domain and the field variable variation.

III.1.1 Galerkin Formulation - The Galerkin finite element formulation begins
with defining the governing differential equation as

$$D_f (f) = 0 \qquad \text{(III.1)}$$

where f signifies the pressure head h for Eq. II.12 and the moisture content θ
for Eq. II.14. The next step in the Galerkin formulation is to approximate
the field variable behavior, i.e.,

$$f \sim \tilde{f} = \Sigma N_i f_i = \lfloor N \rfloor \{f\} \qquad \text{(III.2)}$$

where $\lfloor N \rfloor$ is a row vector of shape or interpolation functions and $\{f\}$ is the
column vector containing the nodal values of the appropriate field variable.

Substituting f from Eq. III.2 into the differential operator of Eq. III.1
gives

$$D_f(\tilde{f}) = R \neq 0 \qquad \text{(111.3)}$$

where R is the residual. If the exact solution f and the approximate solution
$\tilde{f}$ are the same, then the residual of Eq. III.3 would be zero. However, the
approximate solution does not generally equal the exact solution resulting in
the nonzero residual indicated in Eq. III.3. Since the governing differential
equation cannot be satisfied pointwise throughout the domain Ω, its
satisfaction is sought in the sense of a weighted average over the domain   ,
i.e.,

$$\int_\Omega W D_f(\tilde{f}) \, d\Omega = 0 \qquad \text{(III.4)}$$

15

where W is the weighting function.

In the finite element Galerkin formulation, the weighted integral of Eq. III.4 is summed over all the element subdomains Ω^e and the element level shape functions are utilized as the weight functions, i.e.,

$$\int_\Omega WD_f(\tilde{f})\,d\Omega = \sum_{e=1}^{N_e} \int_{\Omega^e} N_j^e \ D_f(\tilde{f})\ d\Omega = 0$$

$$\text{for } j = 1, 2, \ldots, n_e \qquad\qquad (III.5)$$

where N_e is the number of elements used to discretize the domain Ω, N_j^e is the jth shape function for element e and n_e is the number of element shape functions.

The Galerkin formulation of Eq. III.5 possesses the disadvantages of requiring C^1 interelement continuity (i.e., first derivative continuity between the elements), exact satisfaction of all boundary conditions and leads to a nonsymmetric system of equations. These disadvantages can be relaxed or eliminated by generating a 'weak' Galerkin formulation of Eq. III.1. The weak Galerkin formulation is obtained by integrating Eq. III.5 by parts once using the divergence theorem to symbolically give

$$\sum_{e=1}^{N_e} \int_{\Omega^e} N_j^e \ D_f(\tilde{f}^e)\,d\Omega = -\sum_{e=1}^{N_e} \int_{\Omega^e} A(N_j^e)C(\tilde{f}^e)\,d\Omega$$

$$+ \sum_{e=1}^{N_e} \int_{\Gamma^e} \overline{N}_j^e \ B(f^e)\,d\Gamma$$

$$\text{for } j = 1, 2, \ldots, n_e \qquad\qquad (III.6)$$

where $A(\ )$, $C(\ )$ are lower order domain differential operators, $B(\ )$ is a differential operator evaluated along the element boundary Γ^e of Ω^e and $\overline{N}_j^e$ signifies evaluation of N_j^e along Γ^e.

The result of Eq. III.6 for the pressure head analysis (Eq. II.12) is

$$\sum_{e=1}^{N_e} [\int_{\Omega^e} \{N\}(\lfloor \tilde{N} \rfloor \{F(h)\}) \lfloor N \rfloor d\Omega \ \{\dot{h}\}$$

$$+ \int_{\Omega^e} (\lfloor \tilde{N} \rfloor \{K^r(h)\})(\frac{\partial \{N\}}{\partial x} (K^s_{xx} \frac{\partial \lfloor N \rfloor}{\partial x} + K^s_{xy} \frac{\partial \lfloor N \rfloor}{\partial y})$$

$$+ \frac{\partial \{N\}}{\partial y} (K^s_{yx} \frac{\partial \lfloor N \rfloor}{\partial x} + K^s_{yy} \frac{\partial \lfloor N \rfloor}{\partial y})) d\Omega$$

$$+ \int_{\Omega^e} (\lfloor \tilde{N} \rfloor \{K^r(h)\} (\frac{\partial \{N\}}{\partial x} K^s_{xy} + \frac{\partial \{N\}}{\partial y} K^s_{yy}) d\Omega$$

$$- \int_{\Gamma_2^e} \{\overline{N}\} \ q \ d\Gamma] = \{0\} \qquad \text{(III.7a)}$$

and for the moisture content analysis (Eq. II.14) it is

$$\sum_{e=1}^{N_e} [\int_{\Omega^e} \{N\} \lfloor N \rfloor d\Omega \ \{\dot{\theta}\}$$

$$+ \int_{\Omega^e} (\lfloor \tilde{N} \rfloor \{D^r(\theta)\} (\frac{\partial \{N\}}{\partial x} - (K^s_{xx} \frac{\partial \{N\}}{\partial x} + K^s_{xy} \frac{\partial \{N\}}{\partial y})$$

$$+ \frac{\partial \{N\}}{\partial y} (K^s_{yx} \frac{\partial \lfloor N \rfloor}{\partial x} + K^s_{yy} \frac{\partial \lfloor N \rfloor}{\partial y})) d\Omega \ \{\theta\}$$

$$+ \int_{\Omega^e} (\lfloor \tilde{N} \rfloor \{K^r(\theta)\} (\frac{\partial \{N\}}{\partial x} K^s_{xy} + \frac{\partial \{N\}}{\partial y} K^s_{yy}) d\Omega$$

$$- \int_{\Gamma_2^e} \{\overline{N}\} \ q \ d\Gamma] = \{0\} \qquad \text{(III.7b)}$$

where the superposed dot signifies time differentiation and $\{\overline{N}\}$ is the vector
of element shape functions evaluated along the flux loaded element boundary Γ_2^e.

17

The nonlinear material coefficients $F(h)$, $K^r(h)$, $D^r(\theta)$ and $K^r(\theta)$ were spacially approximated using interpolation functions $\lfloor \tilde{N} \rfloor$ and the expressions in braces represent the corresponding nodal values. Note that the interpolation functions $\lfloor \tilde{N} \rfloor$ need not be the same as the interpolation functions $\lfloor N \rfloor$ of Eq. III.2.

Scrutinizing Eqs. III.7(a) and III.7(b) reveals the modifications of the weak Galerkin versus Galerkin formulations. First, the shape functions need only be C^o interelement continuous, i.e, function continuity between the elements. Second, the vector products which multiply the pressure head and moisture content vectors are symmetric which results in a symmetric system of equations. Lastly, only the boundary conditions given by Eqs. II.16(a) and (b) must be exactly satisfied since the flux or flow boundary conditions of Eqs. II.17(a) and (b) are included in the discretized approximation.

Eqs. III.7(a) and (b) can be written in matrix form as

$$[S(h)]\{\dot{h}\} + [K(h)]\{h\} = \{Q(h)\} \qquad \text{(III.8a)}$$

$$[S]\{\dot{\theta}\} + [D(\theta)]\{\theta\} = \{Q(\theta)\} \qquad \text{(III.8b)}$$

where

$$[S(h)] = \sum_{e=1}^{N_e} [S^e(h)]$$

— pressure head dependent flow domain
  storage matrix

$$[S^e(h)] = \int_{\Omega^e} (\lfloor \tilde{N} \rfloor \{F(h)\})\{N\}\lfloor N \rfloor \, d\Omega$$

— element storage matrix

$$[K(h)] = \sum_{e=1}^{N_e} [K^e(h)]$$

18

- pressure head dependent flow domain
  conductivity matrix

$$[K^e(h)] = \int_{\Omega^e} (\lfloor \tilde{N} \rfloor \{K^r(h)\}) \ [\frac{\partial\{N\}}{\partial x} (K^s_{xx} \frac{\partial \lfloor N \rfloor}{\partial x} + K^s_{xy} \frac{\partial \lfloor N \rfloor}{\partial y})$$

$$+ \frac{\partial\{N\}}{\partial y} (K^s_{yx} \frac{\partial \lfloor N \rfloor}{\partial x} + K^s_{yy} \frac{\partial \lfloor N \rfloor}{\partial y})] \ d\Omega$$

- element conductivity matrix

$$\{Q(h)\} = \{Q_p\} + \sum_{e=1}^{N_e} [\int_{\Gamma_2^e} \{\overline{N}\} \ q \ d\Gamma$$

$$- \int_{\Omega^e} (\lfloor \tilde{N} \rfloor \{K^r(h)\}) \ (\frac{\partial\lfloor N \rfloor}{\partial x} K^s_{xy} + \frac{\partial\{N\}}{\partial y} K^s_{yy}) \ d\Omega]$$

- pressure head dependent flow domain
  load vector

$\{Q_p\}$ - applied point source/sink load vector

$$[S] = \sum_{e=1}^{N_e} [S^e]$$

- linear flow domain storage matrix

$$[S^e] = \int_{\Omega^e} \{N\}\lfloor N \rfloor \ d\Omega$$

- element storage matrix

$$[D(\theta)] = \sum_{e=1}^{N_e} [D^e(\theta)]$$

- moisture content flow domain
  diffusivity matrix

$$[D^e(\theta)] = \int_{\Omega^e} (\lfloor \tilde{N} \rfloor \{D^r(\theta)\})$$

$$[\frac{\partial\{N\}}{\partial x} (K^s_{xx} \frac{\partial \lfloor N \rfloor}{\partial x} + K^s_{xy} \frac{\partial \lfloor N \rfloor}{\partial y})$$

$$+ \frac{\partial \{N\}}{\partial y} (K^s_{yx} \frac{\partial \lfloor N \rfloor}{\partial x} + K^s_{yy} \frac{\partial \lfloor N \rfloor}{\partial y})] \ d\Omega$$

— element diffusivity matrix

$$\{Q(\theta)\} = \{Q_p\} + \sum_{e=1}^{N_e} [\int_{\Gamma^e_2} \{\tilde{N}\} \ q \ d\Omega$$

$$- \int_{\Omega^e} (\lfloor \tilde{N} \rfloor \ \{K^r(\theta)\}) \ (\frac{\partial \{N\}}{\partial x} K^s_{xy} + \frac{\partial \{N\}}{\partial y} K^s_{yy}) d\Omega]$$

— moisture content dependent flow
domain load vector

The above element summations are performed by enforcing pressure head or moisture content nodal equilibrium and continuity. This technique is known as direct assembly (e.g., Heubner, 1975).

III.1.2 Element Shape Functions — The next phase in the finite element formulation is to choose the specific finite element(s) to be used in the discretization. As mentioned previously, the quadratic triangular and quadrilateral elements of Fig. III.1 were selected. The shape functions for the six node triangle element are expressed in terms of nondimensional coordinates known as area coordinates. The area (local) coordinate shape functions are (e.g., Zienkiewicz, 1977)

$$N_1 = L_1(2L_1 - 1), \quad N_4 = 4L_1L_2$$

$$N_2 = L_2(2L_2 - 1), \quad N_5 = 4L_2L_3 \qquad \qquad \text{(III.9)}$$

$$N_3 = L_3(2L_3 - 1), \quad N_6 = 4L_3L_1$$

where the element nodes and area coordinates ($0 \leq L_1, L_2, L_3 \leq 1$) are shown in Fig. III.1(a). The three area coordinates are not independent. Thus, in order to utilize an isoparametric formulation of these shape functions, the

coordinate dependence must be removed. The coordinate dependence is easily eliminated by substituting

$$L_3 = 1 - L_1 - L_2$$

into Eq. III.9. The local coordinate shape functions for the eight node quadrilateral element are (e.g., Zienkiewicz, 1977)

$$N_1 = (1-\xi)(1-\eta)(-\xi-\eta-1)/4 \quad , \quad N_5 = (1-\xi^2)(1-\eta)/2$$
$$N_2 = (1+\xi)(1-\eta)(\xi-\eta-1)/4 \quad , \quad N_6 = (1+\xi)(1-\eta^2)/2 \qquad (III.10)$$
$$N_3 = (1+\xi)(1+\eta)(\xi+\eta-1)/4 \quad , \quad N_7 = (1-\xi^2)(1+\eta)/2$$
$$N_4 = (1-\xi)(1+\eta)(-\xi+\eta-1)/4 \quad , \quad N_8 = (1-\xi)(1-\eta^2)/2$$

where the element nodes and nondimensional curvilinear coordinates $\xi, \eta (-1 \leq \xi, \eta \leq 1)$ are shown in Fig. III.1(b).

The material parameter interpolation functions, $\{\tilde{N}\}$, were assumed to be linear. Thus, for the triangular element

$$\tilde{N}_1 = L_1$$
$$\tilde{N}_2 = L_2 \qquad (III.11)$$
$$\tilde{N}_3 = 1-L_1-L_2 \; .$$

and for the quadrilateral element

$$\tilde{N}_1 = (1-\xi)(1-\eta)/4$$
$$\tilde{N}_2 = (1+\xi)(1-\eta)/4 \qquad (III.12)$$
$$\tilde{N}_3 = (1+\xi)(1+\eta)/4$$
$$\tilde{N}_4 = (1-\xi)(1+\eta)/4$$

As shown in Eqs. III.11 and III.12 only the corner nodes for the elements of

21

Fig. III.1 are utilized in describing the element spacial variation of the material coefficients.

III.1.3 <u>Curvilinear</u> <u>Coordinate</u> <u>Transformations</u> – The formulation of element storage, conductivity and diffusivity matrices and the element load vectors, requires differentiation with respect to the x – and y – axes. Since the shape functions for the six node triangle and the eight node quadrilateral are written in local coordinates, a transformation of the coordinates is necessary. The following two-dimensional relationships are used to perform the transformation:

$$
\begin{Bmatrix} \partial N_i / \partial x \\ \partial N_i / \partial y \end{Bmatrix} = [J]^{-1} \begin{Bmatrix} \partial N_i / \partial s \\ \partial N_i / \partial t \end{Bmatrix}
\tag{III.13}
$$

$$
d\Omega = dxdy = |J| dsdt
\tag{III.14}
$$

$$
x = \lfloor N \rfloor \{x\}
\tag{III.15}
$$

$$
y = \lfloor N \rfloor \{y\}
\tag{III.16}
$$

where $[J]$ is the Jacobian matrix; $s,t = L_1$, L_2 for the triangular elements and $s,t = \xi, \eta$ for the quadrilateral elements; and $|J|$ is the Jacobian determinant. The partial derivatives of the element shape functions with respect to s and t can be easily evaluated from Eqs. III.9 and III.10 and therefore will not be presented here.

The Jacobian matrix is constructed from

$$
\frac{\partial N_i}{\partial s} = \frac{\partial N_i}{\partial x} \frac{\partial x}{\partial s} + \frac{\partial N_i}{\partial y} \frac{\partial y}{\partial s}
$$

$$
\frac{\partial N_i}{\partial t} = \frac{\partial N_i}{\partial x} \frac{\partial x}{\partial t} + \frac{\partial N_i}{\partial y} \frac{\partial y}{\partial t}
$$

22

to give

$$\begin{Bmatrix} \partial N_i/\partial s \\ \partial N_i/\partial t \end{Bmatrix} = \begin{bmatrix} \partial x/\partial s & \partial y/\partial s \\ \partial x/\partial t & \partial y/\partial t \end{bmatrix} \begin{Bmatrix} \partial N_i/\partial x \\ \partial N_i/\partial y \end{Bmatrix}$$

$$= \begin{bmatrix} \dfrac{\partial \lfloor N \rfloor}{\partial s}\{x\} & \dfrac{\partial \lfloor N \rfloor}{\partial s}\{y\} \\[2ex] \dfrac{\partial \lfloor N \rfloor}{\partial t}\{x\} & \dfrac{\partial \lfloor N \rfloor}{\partial t}\{y\} \end{bmatrix} \begin{Bmatrix} \dfrac{\partial N_i}{\partial x} \\[2ex] \dfrac{\partial N_i}{\partial y} \end{Bmatrix}$$

$$= \begin{bmatrix} J_{11} & J_{12} \\ J_{21} & J_{22} \end{bmatrix} \begin{Bmatrix} \partial N_i/\partial x \\ \partial N_i/\partial y \end{Bmatrix}$$

$$= [J] \begin{Bmatrix} \partial N_i/\partial x \\ \partial N_i/\partial y \end{Bmatrix} \qquad \text{(III.17)}$$

Therefore, the determinant and inverse of the Jacobian are

$$|J| = J_{11} J_{22} - J_{12} J_{21} \qquad \text{(III.18)}$$

and

$$[J]^{-1} = \frac{1}{|J|} \begin{bmatrix} J_{22} & -J_{12} \\ -J_{21} & J_{11} \end{bmatrix} \qquad \text{(III.19)}$$

The boundary integrals in the evaluation of the element load vector must also be transformed. The transformation of $d\Gamma$ is

$$d\Gamma = J_\Gamma ds \qquad \text{(III.20)}$$

where

$$J_\Gamma = \sqrt{(\partial x/\partial s)^2 + (\partial y/\partial s)^2}$$

23

$$= \sqrt{\left(\frac{d\lfloor \bar{N} \rfloor}{ds} \{x\}\right)^2 + \left(\frac{d\lfloor \bar{N} \rfloor}{ds} \{y\}\right)^2}$$

The analysis now proceeds to the numerical evaluation of the element integrals.

III.1.4   <u>Element Quadrature</u> - Substituting the element shape functions (Section III.1.2) and the curvilinear coordinate transformations (Section III.1.3) into the integrals of Eqs. III.7(a) and (b) would obviously lead to complicated integrands. Consequently, the resulting integrals are numerically evaluated using quadrature formula approximations. In particular, Gaussian quadrature formulas are utilized since high-order integration accuracy can be achieved using a minimum number of function evaluations.

Representing the resulting integrand for a typical triangular element as $I(L_1, L_2)$, the numerical evaluation of the integral is

$$\int I(L_1, L_2) \, dL_1 dL_2 \simeq \sum_{i=1}^{n_g} w_i \, I(L_{1i}, L_{2i}) \tag{III.22}$$

where L_{1i}, L_{2i} are the area coordinates of the i-th sampling point, w_i is the weight associated with the i-th sample point and n_g is the number of Gaussian quadrature points. The weights and sample point area coordinates are given by Cowper (1973). The order of accuracy used to evaluate the integrals of Eq. III.7(a) is fifth or sixth whereas, the integrals of Eq. III.7(b) require only a fourth or fifth order accurate evaluation. If the element is not distorted then the lower order evaluation is used.

The numerical evaluation of the integrals for the quadrilateral elements is

$$\int I(\xi, \eta) \, d\xi d\eta = \sum_{i=1}^{n_g} \sum_{j=1}^{n_g} w_i w_j \, I(\xi_i, \eta_j) \tag{III.23}$$

24

where ξ_i, η_j are the curvilinear coordinates of the i-th and j-th sample points and w_i, w_j are weights associated with the i-th and j-th sample points, respectively. The weights and sample point curvilinear coordinates are the standard Gauss – Legendre quadrature data (e.g., Zienkiewicz, 1977). Equations III.7(a) and (b) are evaluated using n_g = 3 for nondistorted elements and n_g = 4 is typically used for distorted quadrilateral elements. The boundary integrals of Eqs. III.7(a) and (b) are also evaluated using Gauss-Legendre quadrature, i.e.,

$$\int_{\Gamma_2^e} \{\overline{N}(\xi)\} \; q(\xi) \; J_\Gamma d\xi = \sum_{i=1}^{n_g} w \; \{\overline{N}(\xi_i)\} q(\xi_i) \; J_\Gamma(\xi_i) \qquad (III.24)$$

where n_g = 3.

III.2   TEMPORAL DISCRETIZATION

The assembled system of equations describing fluid flow through a soil medium are given in Eqs. III.8(a) and (b). Equations III.8(a) and (b) show that the fluid flow equations require a temporal discretization in addition to the spacial discretization presented in the previous section. In the present investigation a direct single-step numerical time integration scheme is used. The term 'direct' indicates that Eqs. III.8(a) and (b) are not transformed prior to the numerical time integration (Bathe and Wilson, 1976). Direct integration is based on two ideas:

(1)   Satisfaction of the full set of equations at discrete time intervals Δt apart; and

(2)   A variation of the field variable is assumed within each time

25

interval, Δt.

The basis of the single-step scheme is that the filed variable varies linearly in a discrete time interval, Δt, from time t_n to time

$$t_{n+1} = t_n + \Delta t, \quad n \varepsilon \ 0,1,\ldots, N_t \qquad \text{(III.25)}$$

where N_t is the number of time steps. Evaluating Eqs. III.8(a) and (b) at $t_n + \delta \Delta t$ $(0 \leq \delta \leq 1)$ gives

$$[S(h_{n+\delta})] \ \{\dot{h}\}_{n+\delta} + [K(h_{n+\delta})] \ \{h\}_{n+\delta}$$

$$= \{Q(h_{n+\delta})\}_{n+\delta} \qquad \text{(III.26a)}$$

$$[S]\{\dot{\theta}\}_{n+\delta} + [K(\theta_{n+\delta})] \ \{\theta\}_{n+\delta}$$

$$= \{Q(\theta_{n+\delta})\}_{n+\delta} \qquad \text{(III.26b)}$$

Using the linear time approximation of Fig. III.2 leads to (Damjanic and Owen, 1982)

$$\{\dot{h}\}_{n+\delta} = (\{h\}_{n+\delta} - \{h\}_n)/\delta\Delta t \qquad \text{(III.27)}$$

$$\{h\}_{n+\delta} = \delta \{h\}_{n+1} + (1-\delta)\{h\}_n \qquad \text{(III.28)}$$

with a similar result for the moisture content. Substituting Eq. III.27 into Eq. III.26(a) gives

$$(\frac{1}{\delta\Delta t} \ [S(h_{n+\delta})] + [K(h_{n+\delta})])\{h\}_{n+\delta}$$
$$= \{Q(h_{n+\delta})\}_{n+\delta} + \frac{1}{\delta\Delta t} \ [S(h_{n+\delta})]\{h\}_n \qquad \text{(III.29)}$$

Equation III.29 is utilized to obtain $\{h\}_{n+\delta}$ and the pressure head at time

t_{n+1} is obtained from Eq. III.28, i.e.,

$$\{h\}_{n+1} = (1/\delta)\{h\}_{n+\delta} + (1 - 1/\delta)\{h\}_n \qquad \text{(III.30)}$$

Hughes (1977) has shown that the single-step time integration scheme is unconditionally stable when $\delta \geq 1/2$ for both linear and nonlinear situations. Consequently, the present investigation is limited to $1/2 \leq \delta \leq 1$; in particular the work focuses on $\delta = 1/2$, the Crank-Nicolson scheme.

A disadvantage of using time integration schemes with $1/2 \leq \delta < 1$ is that the time increment must be limited to produce an oscillation free solution (e.g., Wood and Lewis, 1975). Blandford and Tauchert (1984) present a modification to the basic single-step time discretization strategy which dampens the oscilliatory noise. The modified scheme is obtained by satisfying Eq. III.29 at time $t_0 + \delta\Delta t$ for the first time step only without extending the solution to the end of the full time step (i.e., $\{h\}_1$ via Eq. III.30 is not calculated). This is equivalent to employing an Euler-backward difference scheme ($\delta=1$) for the first time step but for $\Delta t_1 = \delta\Delta t$ (note, for $\delta=1$ the solution does not oscillate). After the first step the standard scheme (Eqs. III.29 and III.30) is used over the full time step.

III.3 NONLINEAR ANALYSIS

The discretized saturated-unsaturated subsurface flow equation (Eq. III.29) is nonlinearly dependent on the pressure head (similarly, the θ-based discretized equation is dependent on the moisture content). Thus, procedures are required to approximate the nonlinear material properties and solve the resulting nonlinear simultaneous equations. This section discusses the representation of the nonlinear material data, the iterative solution strategy and the incorporation of nonlinear boundary conditions.

III.3.1 __Nonlinear__ __Material__ __Property__ __Representation__ – Equation III.29 includes

the moisture content, θ, and the relative hydraulic conductivity, K^r, pressure

head dependent material parameters. The variation of the specific moisture

capacity, $(d\theta/dh)$, can be obtained from the θ versus h relationship. A typical

graph depicting the relationships $\theta(h)$ and $K^r(h)$ are shown in Fig. III.3.

The process of subsurface groundwater flow is comprised of a succession

of wetting and drying of the soil medium. The wetting/drying process results

in hysteretic behavior as shown in Fig. III.3. The numerical model of this

investigation assumes that the material relationships are single valued

functions in terms of h or θ (i.e., $\theta(h)$, $K^r(h)$, $D^r(\theta)$ and $K^r(\theta)$).

Consequently, the hysteresis between wetting and drying conditions in the soil

medium layers is neglected. Obviously, the assumption is correct if the soil

medium is uniformly wetting (infiltration) or uniformly drying (drainage) as

shown in Fig. III.3. For simultaneous wetting/drying an average curve should

be used.

Generally, the nonlinear material property data is available in tabular

form. The values are listed using regular/irregular increments in pressure

head or moisture content. Once the nonlinear material data has been obtained

in tabular form, the material parameter relationships must be numerically

represented in order to perform an analysis. Various techniques, which

represent different levels of accuracy, can be used, e.g., (i) linear

interpolation within each interval of the table, (ii) an approximate analytic

fit to the tabulated data, or (iii) cubic spline interpolation.

Linear interpolation has an obvious drawback in accuracy if the data is

tabulted at large intervals. Approximate analytic fits, for nonlinear

material properties in groundwater flow problems, have been suggested by Moore (1981) but were found unsuitable for general use. Consequently, the cubic spline interpolation routines available in the IMSL (1982) package were used.

Cubic spline interpolation involves the passage of a piecewise smooth cubic polynominal through the data points of a nonlinear relationship. Cubic splines have a continuous second order derivative, which makes the interpolation smooth. The physical nature of the nonlinear relationships requires the specification of the first derivative values at the table entry extremes. For example, in Fig. III.3 the graph becomes asymptotic to a vertical line which marks a minimum value of moisture content (irreducible water saturation) for any soil medium. The value of the first derivative, when θ equals its value at minimum saturation, is specified to be zero. The slope of the curve, θ vs. h, at saturation varies according to the type of soil being tested, and should be specified accordingly. The values of the first derivative for the nonlinear relationship between K and h are specified according to the data for a particular soil. The piecewise smooth, continuous second order derivative, interpolation of θ vs. h, facilitates the evaluation of $d\theta/dh$. It may be noted, that the interpolation of specific moisture capacity, $d\theta/dh$ is continuous through first order differentiation. The cubic spline interpolation of $D^r(\theta)$ and $K^r(\theta)$ is essentially the same as for $\theta(h)$ and $K^r(h)$. Consequently, no specific details need to be provided.

III.3.2 <u>Nonlinear Solution Strategy</u> – Various nonlinear solution strategies are available for solving Eq. III.29, e.g., (i) direct iteration, (ii) Newton-Raphson iteration and (iii) modified Newton-Raphson iteration. Each iteration strategy is based on a repeated formulation and solution of a linear system of equations. Newman (1973) recommended the direct iteration scheme for the

solution of saturated-unsaturated subsurface flow problems. Consequently, the direct iteration strategy was utilized in the present investigation.

The direct iteration strategy for Eq. III.29 can be written as

$$\left(\frac{1}{\delta \Delta t} [S(h_{n+\delta}^i)] + [K(h_{n+\delta}^i)] \right) \{h\}_{n+\delta}^{i+1}$$

$$= \{Q(h_{n+\delta}^i)\}_{n+\delta} + \frac{1}{\delta \Delta t} [S(h_{n+\delta}^i)] \{h\}_n$$

$$\text{for } i = 0, 1, 2, \ldots \qquad (III.31)$$

where superscript i is the iteration number and $h_{n+\delta}^O$ is approximated using linear extrapolation, i.e.,

$$h_{n+\delta}^O = (1 + \delta) h_n - \delta h_{n-1}$$

The iteration via Eq. III.31 is continued until

$$\left| \frac{h_{n+\delta}^{i+1} - h_{n+\delta}^i}{h_{n+\delta}^{i+1}} \right| < \varepsilon \qquad (III.32)$$

where ε is a prescribed tolerance (generally choose 1×10^{-3}) or until the number of user specified interations is equalled. The iteration strategy for the θ-based unsaturated subsurface flow equation is

$$\left(\frac{1}{\delta \Delta t} [S] + [D(\theta_{n+\delta}^i)] \right) \{\theta\}_{n+\delta}$$

$$= \{Q(\theta_{n+\delta}^i)\}_{n+\delta} + \frac{1}{\delta \Delta t} [S] \{\theta\}_n$$

$$\text{for } i = 0, 1, 2, \ldots \qquad (III.33)$$

The convergence criteria is the same as Eq. III.32, simply replace h with θ.

A schematic of the direct iteration strategy is shown in Fig. III.4. Figure III.4 depicts the fact that several matrix assemblies (see Eqs. III.8) and subsequent solutions (Eq. III.31 or III.33) are required to obtain a convergent solution. Consequently, an efficient assembly and equation solving scheme should be utilized. These equations are assembled consistent with Gauss-Crout elimination algorithm of Taylor (1977). Taylor's skyline solution algorithm incorporates the symmetry of the equations and sparseness of the resulting finite element equations. Thus, the storage of the matrix coefficients and the matrix decomposition and back substitution operations are minimized.

III.3.3 __Nonlinear Boundary Conditions__ - This section discusses the boundary conditions on seepage and evaporation/infiltration surfaces. These surfaces represent nonlinear boundary conditions because they can alternate between the conditions given by Eqs. II.16 and II.17.

A seepage face (surface) is an external boundary of the saturated zone where water leaves the system and h is uniformly zero. Unfortunately, the length of the seepage face varies with time in a manner that cannot be predicted apriori. Neuman (1973) devised a scheme to incorporate the changing length of the seepage face. Neuman's scheme involves considering all nodes which can belong to a seepage face by having zero values of h_n and negative values of q_n (q_n is negative when the flow at node n is directed out of the system). Now assume that the position of the seepage face is known at time t_k and it is desired to predict the seepage face position at time t_{k+1}. During the first iteration (i=0), h is prescribed to equal zero (pressure head boundary; Eq. II.16(a)) along the initial seepage face. At the same time, q

is prescribed to equal zero (flux boundary; Eq. II.17(a)) at all seepage nodes where h < 0. The solution should produce negative q values at nodes where h is zero and negative h values at nodes where q is prescribed zero. However, if a positive value of q is encountered at an h = 0 node, the value of q is set to zero for the next iteration. Similarly, if a positive h value is obtained at a q = 0 node, then h is prescribed to be zero for the next iteration.

Neuman (1973) found that the boundary condition modifications should proceed sequentially from node to node starting at the saturated end of the seepage face. In addition, after having set q equal to zero at any node during a given iteration, q at all subsequent nodes must also be set equal to zero. The iterative solution procedure for the seepage face continues in the same manner as described in the previous section.

The evaporation/infiltration surface is that part of the external boundary where the soil can lose water to the atmosphere by evaporation or gain water by infiltration due to rainfall or sprinkler irrigation. The potential rates for both evaporation and infiltration are governed by atmospheric conditions. However, the ability of the porous medium to transmit or absorb moisture is limited by the medium composition. Thus, the exact boundary conditions at the soil surface cannot be predicted apriori.

Neuman (1975) suggested the following requirements for the evaporation/infiltration boundaries

$$\left| (K^r(h)\overline{\overline{K}}^s \nabla (h+Z)) \cdot \overline{n} \right| \leq \left| V_p \right| \tag{III.34}$$

$$h_L \leq h \leq 0 \tag{III.35}$$

where V_p is the prescribed potential flux and h_L is the minimum allowed

pressure head at the soil surface. Equation III.35 states that, in the absence of water accumulation at the soil surface, h is limited by h_L from below and by atmospheric pressure from above (Neuman, 1975). The lower limit, h_L, can be determined from equilibrium conditions between the soil water and atmospheric vapor (e.g., Rose, 1966, p. 157).

Neuman (1975) suggested the following scheme for incorporating Eqs. III.34 and III.35. During the first iteration in each time step, the surface nodes are treated as a prescribed flux boundary (Eq. II.17(a)) and are assigned an arbitrary fraction of the potential flux, usually 0.10. If the computed values of h_n satisfy Eq. III.35, then the flux at each node n is increased by $|h_L|/|h_n|$ in the case of evaporation, or by $|h_L|/|h_L-h_n|$ in the case of infiltration, subject to Eq. III.34. If some value of h_n lies outside the limits specified by Eq. III.35 then, during the subsequent iteration, node n is treated as a prescribed pressure head node with $h = h_L$ for evaporation and $h = 0$ for infiltration. This situation is maintained as long as Eq. III.34 is satisfied. If, at any stage of the computation, the calculated flux exceeds the potential flux such that Eq. III.34 is not satisfied, node n is assigned the potential flux and is treated as a prescribed flux boundary.

The adaptation of Eqs. III.34 and III.35 for a partially saturated moisture content analysis is

$$|\overline{\overline{K}}^s(D^r(\theta)\nabla\theta + K^r(\theta)\nabla Z)\cdot\overline{n}| \le V_p \qquad (III.36)$$

$$\theta_R \le \theta \le \theta_s \qquad (III.37)$$

where θ_R is the irreducible moisture content and θ_s is the saturated moisture content. The discussion following Eqs. III.34 and III.35 is also applicable to Eqs. III.36 and III.37.

The iteration procedure discussed in the previous section is again applicable to the evaporation/infiltration boundary conditions. Iteration continues until convergence is achieved or the number of iterations is exceeded.

III.4   VELOCITY SMOOTHING

The finite element formulations presented earlier yield nodal pressure head or moisture content values. As shown in Section III.3.3, the seepage and evaporation/infiltration boundaries require the calculation of the Darcian velocities. Furthermore, the local Darcian velocities are required for the analysis of groundwater pollutant dispersion.

The Darcian velocities are calculated using

$$\begin{Bmatrix} V_x \\ V_y \end{Bmatrix} = -K^r(h) \begin{bmatrix} K^s_{xx} & K^s_{xy} \\ K^s_{yx} & K^s_{yy} \end{bmatrix} \left(\begin{Bmatrix} \partial h/\partial x \\ \partial h/\partial y \end{Bmatrix} + \begin{Bmatrix} 0 \\ 1 \end{Bmatrix} \right) \tag{III.38a}$$

or

$$\begin{Bmatrix} V_x \\ V_y \end{Bmatrix} = - \begin{bmatrix} K^s_{xx} & K^s_{xy} \\ K^s_{yx} & K^s_{yy} \end{bmatrix} \left(D^r(\theta) \begin{Bmatrix} \partial \theta/\partial x \\ \partial \theta/\partial y \end{Bmatrix} + K^r(\theta) \begin{Bmatrix} 0 \\ 1 \end{Bmatrix} \right) \tag{III.38b}$$

Equations III.38(a) and (b) show that the Darcian velocity calculations involve derivatives of the field variable (pressure head or moisture content). The elements selected for calculating the field variable nodal values are only C^0 interelement continuity. Thus, the Darcian velocities are generally discontinuous between the elements.

Hinton and Campbell (1974) have presented smoothing techniques to reduce interelement velocity discontinuities. Generating a least squares smoothing

over the finite element mesh results in the "global" smoothing procedure. Alternatively, the smoothing process may be performed separately over each individual element and is referred to as "local" smoothing. Fig. III.5 is a schematic showing the results of global and local smoothing. As shown in Fig. III.5, global smoothing results in a continuous velocity field. The disadvantage of global smoothing is its computational expense. Thus, local smoothing is utilized in this study.

The local integral least squares smoothing is based on first evaluating Eq. III.38(a) or Eq. III.38(b) at the Gauss quadrature points. The quadrature points are utilized because integration point evaluations are one order more accurate than other points within the domain (Zienkiewicz, 1977). The nodes, which are the most useful output locations, appear to be the worst sampling points. An explanation for this observed phenomenum is that the interpolation functions tend to behave badly near the extremities of the interpolation region.

The next step is to define the residual between the smoothed velocities, $\tilde{V}$ and the quadrature point velocites, V, i.e.,

$$R = \int_{\Omega^e} (\tilde{V} - V)^2 \, d\Omega \qquad (III.39)$$

The variation of $\tilde{V}$ is taken to be

$$\tilde{V} = \lfloor \tilde{N} \rfloor \{V\} \qquad (III.40)$$

where $\{\tilde{V}\}$ is the of smoothed velocities at the element corner nodes and the shape functions $\{\tilde{N}\}$ are given in Eq. III.11 for the triangular elements and in Eq. III.12 for the quadrilateral elements. Substituting Eq. III.40 into Eq. III.39 gives

$$R = \int_{\Omega^e} (\lfloor \tilde{N} \rfloor \{\tilde{v}\} - v)^2 \, d\Omega \qquad \text{(III.41)}$$

Minimizing the residual of Eq. III.41 with respect to $\lfloor \tilde{v} \rfloor$ leads to

$$\frac{\partial R}{\partial \lfloor \tilde{v} \rfloor} = \{0\} = \int_{\Omega^e} (\{\tilde{N}\} \lfloor \tilde{N} \rfloor \{\tilde{v}\} - \{\tilde{N}\} v) d\Omega \qquad \text{(III.42)}$$

Using Gaussian quadrature (Section III.1.4) to evaluate Eq. III.42 results in

$$(\sum_{i=1}^{n_g} w_i \{\tilde{N}(L_{1i}, L_{2i})\} \lfloor \tilde{N}(L_{1i}, L_{2i}) \rfloor \mid J(L_{1i}, L_{2i}) \mid) \{\tilde{v}\}$$

$$= \sum_{i=1}^{n_g} w_i \{\tilde{N}(L_{1i}, L_{2i})\} \mid J(L_{1i}, L_{2i}) \mid v(L_{1i}, L_{2i}) \qquad \text{(III.43)}$$

for the triangular element and

$$(\sum_{i=1}^{n_g} \sum_{j=1}^{n_g} w_i w_j (\{\tilde{N}(\xi_i, \eta_j)\} \lfloor \tilde{N}(\xi_i, \eta_j) \rfloor \mid J(\xi_i, \eta_j) \mid) \{\tilde{v}\}$$

$$= \sum_{i=1}^{n_g} \sum_{j=1}^{n_g} w_i w_j \{\tilde{N}(\xi_i, \eta_j)\} \mid J(\xi_i, \eta_j) \mid v(\xi_i, \eta_j) \qquad \text{(III.44)}$$

for the quadrilateral elements. Equations III.43 and III.44 can be written matrix form as

$$[S_t^e]\{\tilde{v}_t\} = \{r_t\} \qquad \text{(III.45)}$$

and

$$[S_q^e]\{\tilde{v}_q = \{r_q\} \qquad \text{(III.46)}$$

where subscript t is used to signify triangular element and subscript q to signify quadrilateral element. The matrix $[S^e]$ is the symmetric velocity smoothing matrix and $\{r\}$ is the right hand side vector. Once the corner node velocities are obtained from Eq. III.45 or III.46, the midside velocity values are obtained using linear interpolation.

36

Global Coordinates   Local Coordinates
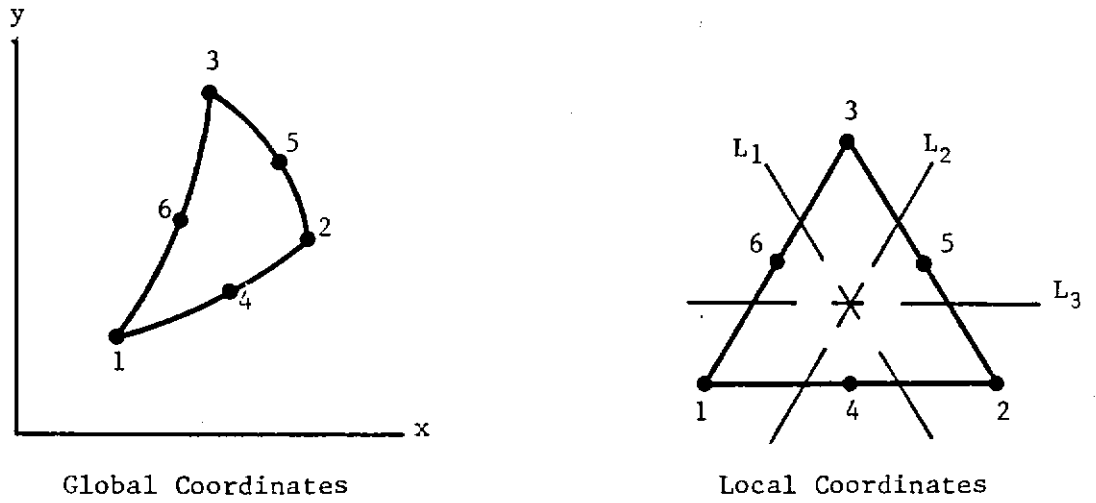
(a) Isoparametric Six Node Triangle

$(0 \leqslant L_1, L_2, L_3 \leqslant 1)$

Global Coordinates   Local Coordinates
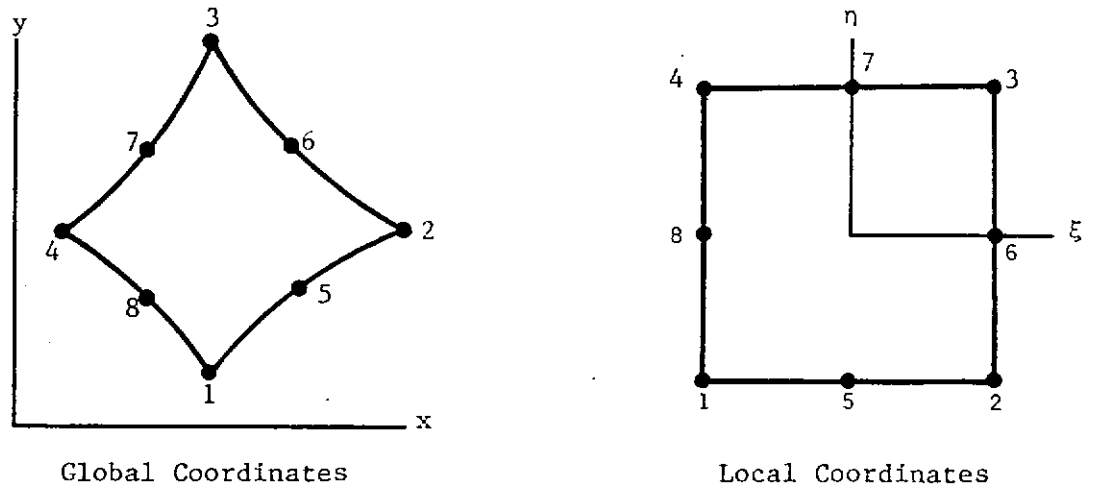
(b) Isoparametric Eight Node Quadrilateral

$(-1 \leqslant \xi, \eta \leqslant 1)$
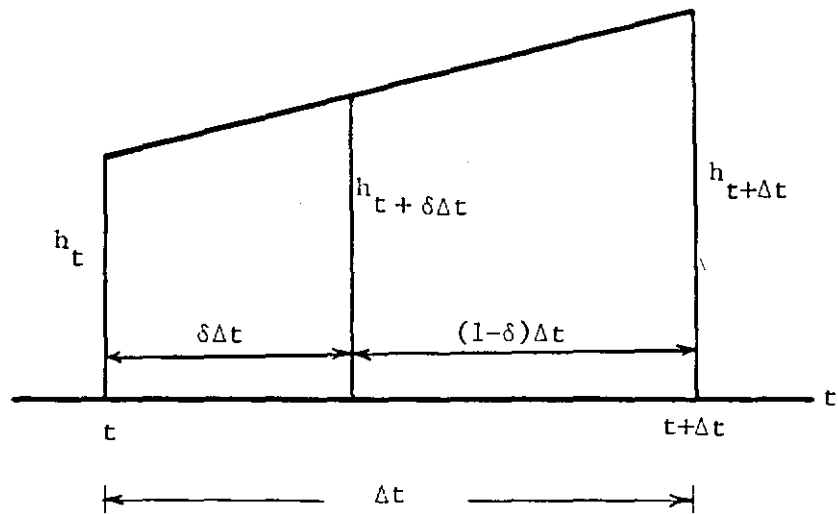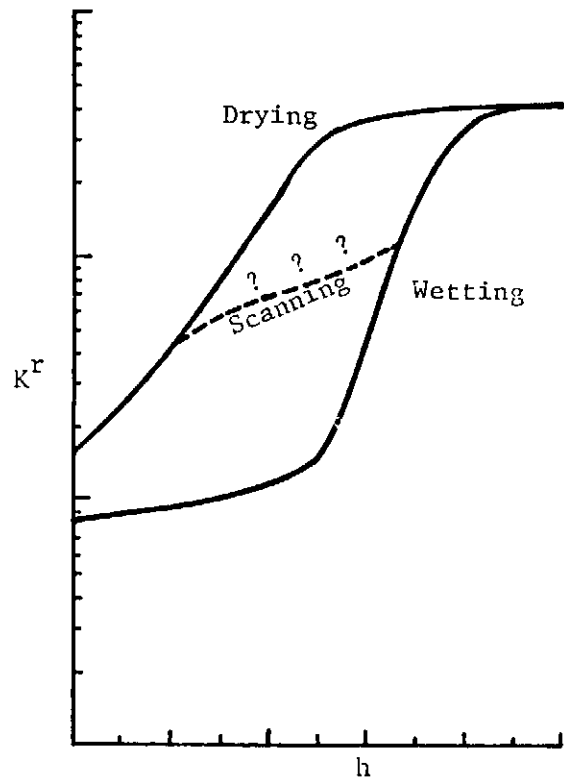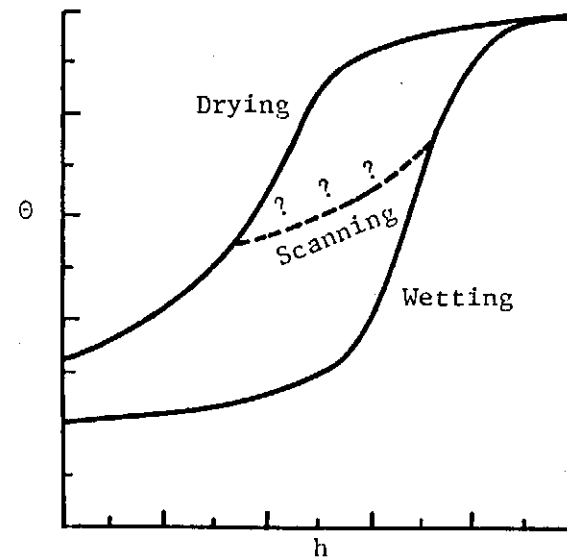
FIG. III.1 – QUADRATIC FINITE ELEMENTS

FIG. III.2 - LINEAR TIME INTERPOLATION SCHEME

(a) Relative Hydraulic Conductivity
    vs Pressure Head Curves

(b) Moisture Content vs
    Pressure Head Curves

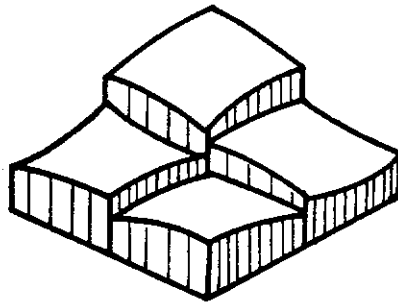FIG. III.3 - SCHEMATIC HYDRAULIC CONDUCTIVITY AND MOISTURE CONTENT CURVES
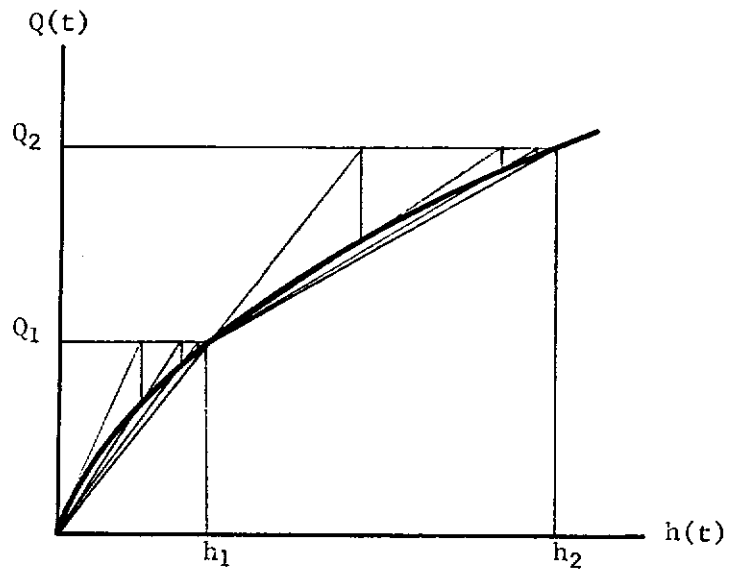
FIG. III.4 – SCHEMATIC OF THE DIRECT ITERATION STRATEGY
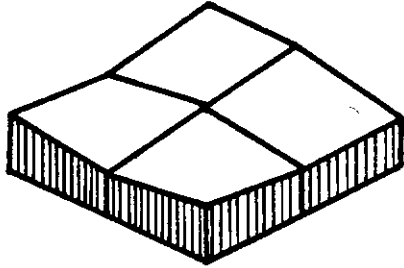
(a) Glabally Smoothed Velocities
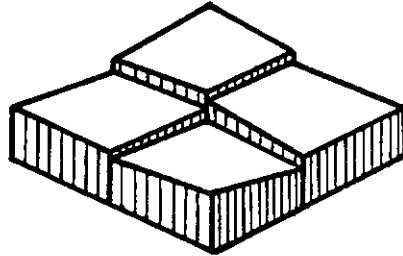
(b) Locally Smoothed Velocities

(c) Unsmoothed Velocities

FIG. III.5 – SCHEMATIC OF DARCIAN VELOCITIES

41

CHAPTER IV

NUMERICAL RESULTS

Several numerical simulations are presented in this chapter illustrating various aspects of the developed model. Both steady state and transient results are presented.

IV.1 STEADY STATE SIMULATION

The first problem deals with the steady state solution of nonlinear one-dimensional aquifer problem using two-dimensional finite element meshes. The differential equation is

$$\frac{d}{dx} k(h)\frac{dh}{dx} = 0 \text{ for } 0<x<1 \tag{IV.1}$$

subject to the boundary conditions

$$\frac{dh}{dx}(x = 0) = 0.0 \tag{IV.2}$$

$$h(x = 1) = 1.0$$

The problem posed by Eqs. IV.1 and IV.2 was solved using $k(h) = k_0$, a constant (linear) and for $k(h) = k_0(1+h)$, a linear function of the pressure head (nonlinear). Both triangular and quadrilateral finite element meshes were used as shown in Fig. IV.1. The finite element results are compared with the exact results in Table IV.1. The exact nonlinear solution was obtained from Tauchert (1977). As shown in Table IV.1 the finite element results are exact for the linear analysis case and nearly exact for the nonlinear analysis case.

IV.2 LINEAR TRANSIENT SIMULATIONS

Two linear transient simulations are presented which involve solving the partial differential equation

$$K_{xx}^S \frac{\partial^2 h}{\partial x^2} + K_{yy}^S \frac{\partial^2 h}{\partial y^2} = \frac{\partial h}{\partial t} \; ; \; 0 \leq x,y \leq 1 \; ; \; t \geq 0 \qquad (IV.3)$$

subject to the initial and boundary conditions

$$h(x,y,o) = 0$$

$$h(1,y,t) = h(x,1,t) = 1 \qquad (IV.4)$$

$$\frac{\partial h}{\partial x}(0,y,t) = \frac{\partial h}{\partial y}(x,o,t) = 0$$

The exact solution to Eqs. IV.3 and IV.4 as given by Bruch and Zyvolski (1974) is

$$h(x,y,t) = 1 + \sum_{n=1}^{\infty} \sum_{m=1}^{\infty} C_{nm} \left[\cos (2n-1) x/2 \right] \cos \left[(2m-1) y/2 \right]$$

$$\exp\{-\pi^2 t \left[K_{xx}^S (2n-1)^2 + K_{yy}^S (2m-1)^2 \right]/4\} \qquad (IV.5)$$

where

$$C_{nm} = - \frac{16(-1)^{n+1} (-1)^{m+1}}{\pi^2 (2n-1)(2m-1)}$$

Physically, this problem may represent the rise of hydraulic head in an infinite othotropic porous medium of square cross section and having compressive capacity of unity (Narasimhan, Neuman and Edwards, 1977). Two cases with different ratios between K_{xx}^S and K_{yy}^S are considered in the following subsections.

IV.2.1 Isotropic Case − The first case is that of an isotropic medium, i.e., $K_{xx}^S = K_{yy}^S = 1$. The finite element mesh for this case is shown in Fig. IV.2. Only one-half of the domain needs to be discretized due to the symmetry of the problem. The boundary condition along the line of symmetry is $\frac{\partial h}{\partial n} = 0$, i.e., a

no flow boundary.

The time history results at nodes 25 and 14 are shown in Figs. IV.3 and IV.4, respectively using a $\Delta t = 0.02$ and $\delta = 1/2$. i.e., Crank-Nicolson (CN) scheme. Figure IV.3 shows the oscillatory behavior of the Crank-Nicholson scheme near the prescribed pressure head boundry whereas Fig. IV.4 reveals that the finite element solution does not tend to oscillate in the interior of the mesh. There are several techniques available to reduce the ocillatory noise near the boundaries, e.g., (1) refine the mesh near the boundary which would increase the number of unknown variables, (2) use backward differencing which would decrease overall solution accuracy, etc. A simple and accurate technique was developed by Blandford and Tauchert (1984) to reduce the oscilliatory noise. As mentioned in Chapter III, the technique is based on first solving the discretized equations at time $\delta \Delta t$ using backward differencing and then using the full time step with the appropriate δ for all subsequent time steps. These "modified" results lead to less oscillatory noise as shown by the modified Crank-Nicolson (MCN) results of Fig. IV.3.

IV.2.2 <u>Orthotropic</u> <u>Case</u> - The second case is an orthotropic medium with $K_{xx}^{s} = 1$ and $K_{yy}^{s} = 100$. The finite element mesh for the orthotropic aquifer case is shown in Fig. IV.5. A full domain discretization is required for this case since the pressure head response is not symmetric with respect to the line $x = y$.

The time histories at nodes 49 and 33 are shown in Figs. IV.6 and IV.7, respectively. The time histories were obtained using Crank-Nicolson and modified Crank-Nicolson time integration schemes with a $\Delta t = 0.001$. A smaller Δt is required due to the orthotropic conductivity properties. Figure IV.6 shows that the modified Crank-Nicolson scheme reduces the oscillatory noise near the boundaries for the orthotropic case as well. Figure IV.6 also shows

that the initial finite element simulation is not particularly accurate. This is due to the strong y-axis hydraulic conductivity relative the the x-axis hydraulic conductivity. A more refined mesh along the x-axis would eliminte this problem. Only the Crank-Nicolson results are presented for interior node 33 as shown in Fig. IV.7. The modified Crank-Nicolson results for node 33 would be exactly the average of the Crank-Nicolson results for the linear simulation.

IV.3 NONLINEAR TRANSIENT SIMULATION

The nonliner transient simultion is infiltration into a soil slab (Burch, 1976) is shown schematically in Fig. IV.8(a). The slab consists of initially air-dry homogeneous soil, Pachappa Loam, underlain by a horizontal impervious barrier along ED. The water source is along BC and is assumed to be maintained at $\Theta_s = 0.330$. The relaive soil-moisture diffusivity is

$$D^r(\theta) = 0.00125 \ \exp(27.8\theta) \ cm^2/min \tag{IV.6}$$

and the relative hydraulic conductivity is

$$K^r(\theta) = 0.00625 \left(\frac{\theta-0.04}{\theta-0.04}\right)^6 \ cm/min \tag{IV.7}$$

in which $\Theta_R = 0.04$ is the irreducible moisture content. The relative soil-moisture diffusivity and the relative hydraulic conductivity were approximated using cubic spline interpolation of the exact function values and end slopes for $0.04 \leq \theta \leq 0.33$ in increments of $\Delta\theta = 0.01$. The saturated hydraulic conductivities are $K^S_{xx} = K^S_{yy} = K^S = 1$ and $K^S_{xy} = 0$.

The partial differential equation given by Eq. II.14 governs the soil slab infiltration problem subjected to the initial and boundary conditions

$$\Theta(\overline{X},0) = \Theta_0 = 0.10 \tag{IV.8}$$

45

$$\Theta = \Theta_s \text{ along BC} \tag{IV.9a}$$

$$\frac{\partial \Theta}{\partial x} = 0 \text{ along CD and EA} \tag{IV.9b}$$

$$D^r(\Theta)K^s \frac{\partial \Theta}{\partial y} + K^r(\Theta)K^s = 0 \text{ along AB and DE} \tag{IV.9c}$$

A quadratic interpolation was used for line BC, i.e.,

$$y_{BC} = -x^2_{BC}/48 + x_{BC}/3 \tag{IV.10}$$

where point B is the origin for Eq. IV.10.

The finite element mesh for the soil slab infiltration analysis is shown in Fig. IV.8(b). The moisture content contours are plotted for t = 10 min and t = 20 min in Fig. IV.8(a). These moisture content contours were obtained using the Crank-Nicolson scheme with Δt = 0.40 min. The finite element integrations of Chapter III were performed using n = 3. The results of Fig. IV.8(a) compare favorably with the results of Burch (1976). The inexact comparison is due to the slightly different boundary conditions utilized by Burch along AB and DE.

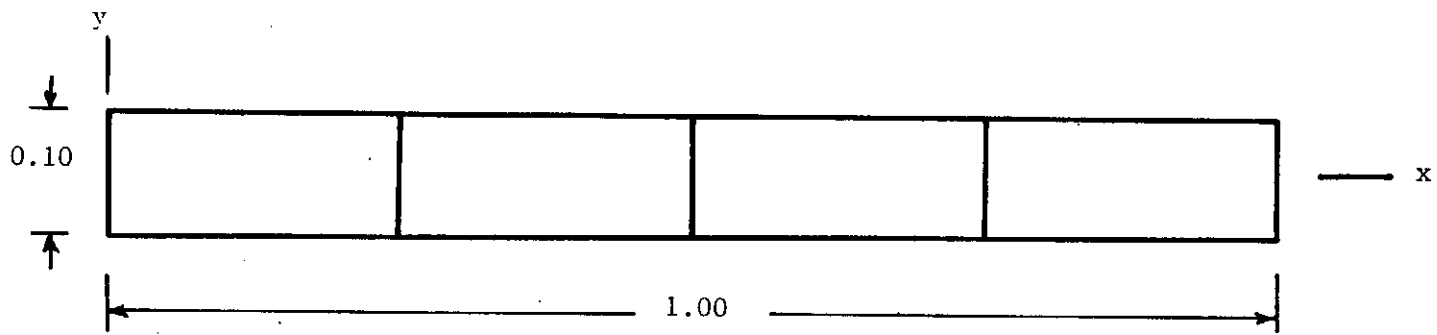TABLE IV.1 – ONE-DIMENSIONAL STEADY-STATE

PRESSURE HEAD RESULTS

	Linear			Nonlinear		
x	Exact[1]	FEM Triangle	FEM Quadrilateral	Exact[2]	FEM Triangle	FEM Quadrilateral
0.25	0.250	0.250	0.250	0.323	0.324	0.324
0.50	0.500	0.500	0.500	0.581	0.582	0.582
0.75	0.750	0.750	0.750	0.803	0.803	0.803
1.00	1.000	1.000	1.000	1.000	1.000	1.000

[1]$h = x$

[2]$h = \sqrt{1+3x} - 1$
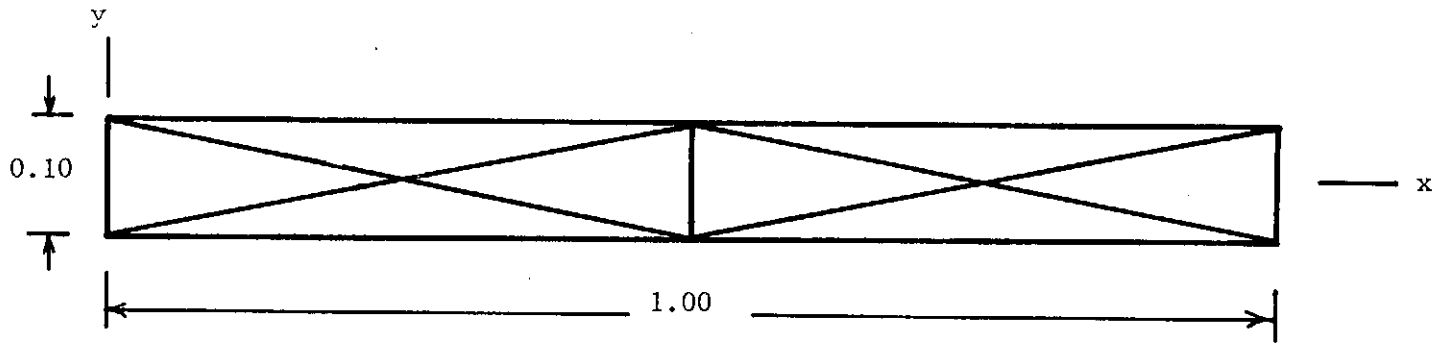
(a)   Triangular Element Mesh

(b)   Quadrilateral Element Mesh

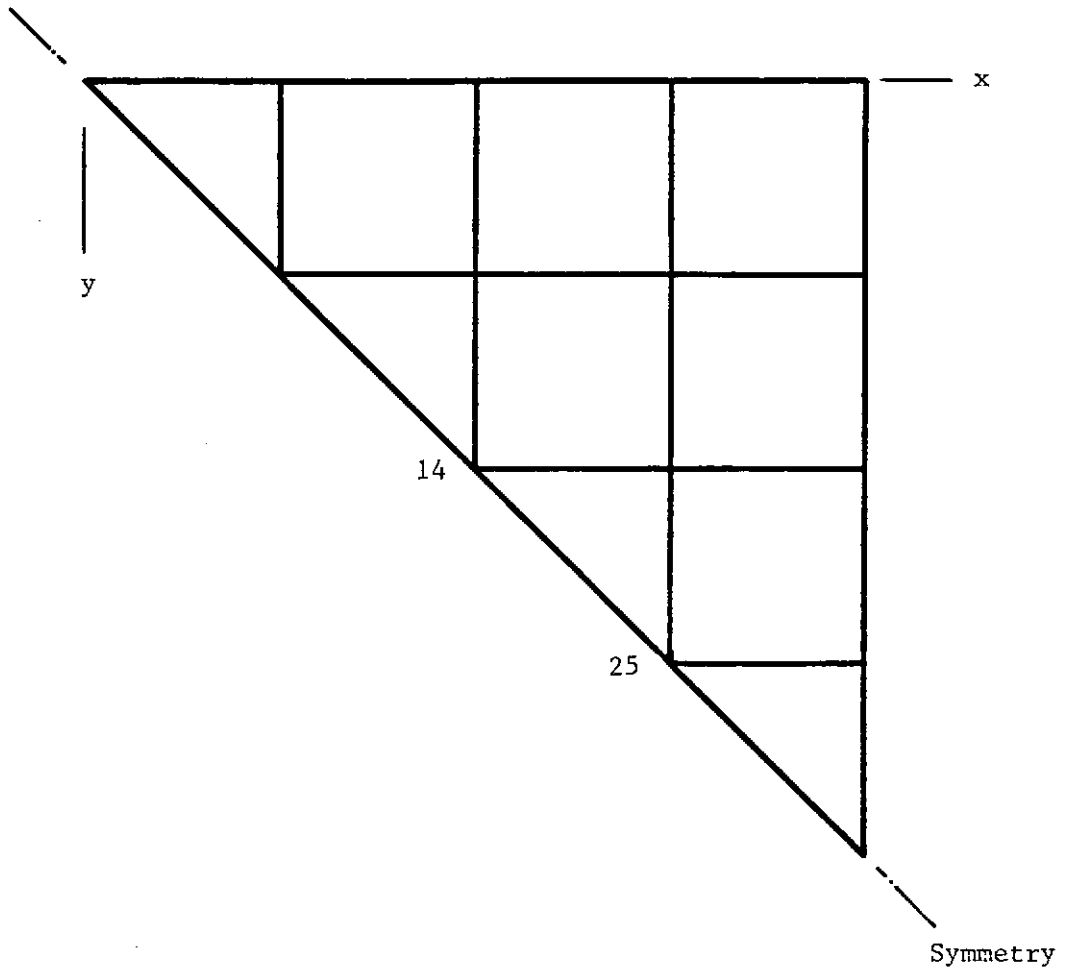FIG. IV.1 - ONE-DIMENSIONAL STEADY STATE FINITE ELEMENT
DISCRETIZATIONS

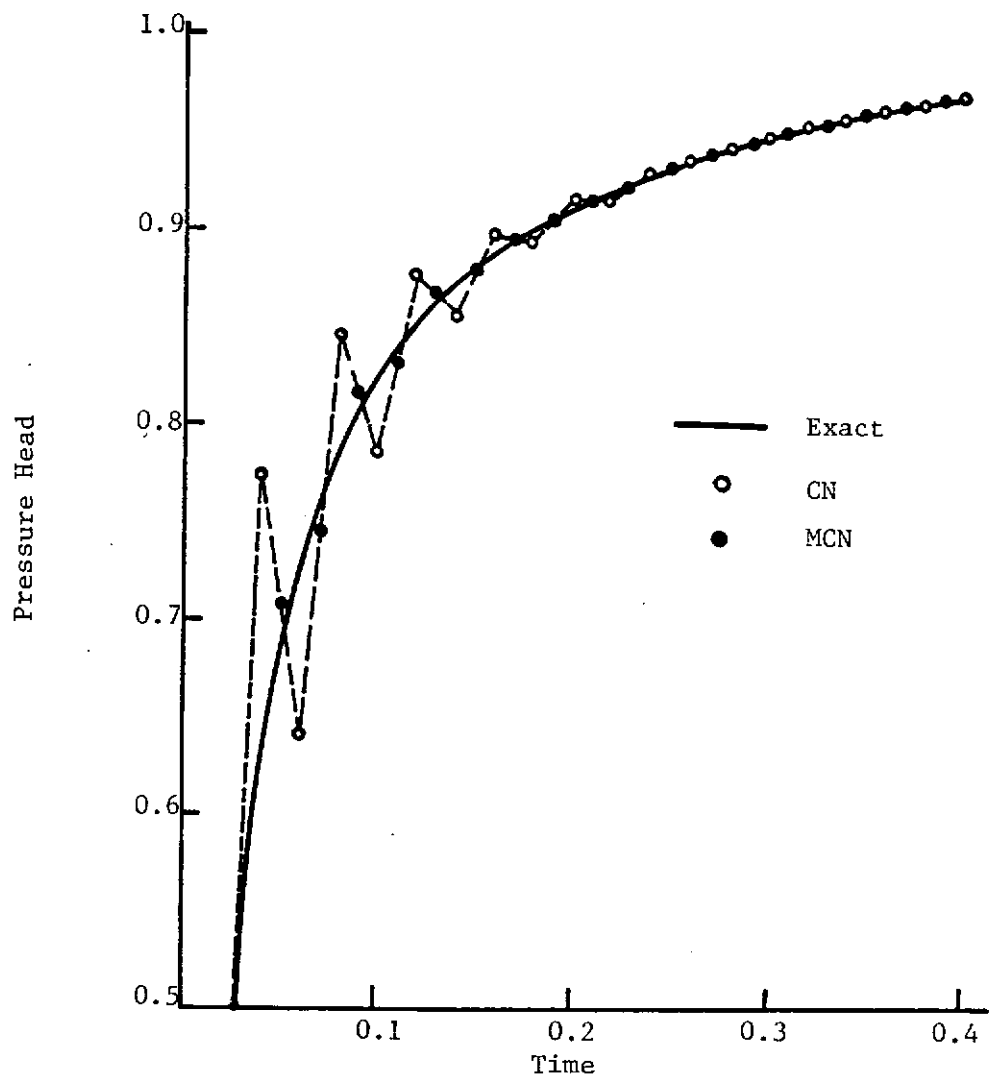FIG. IV.2 - FINITE ELEMENT MESH FOR THE
ISOTROPIC AQUIFER ANALYSIS

FIG. IV.3 - ISOTROPIC AQUIFER PRESSURE HEAD
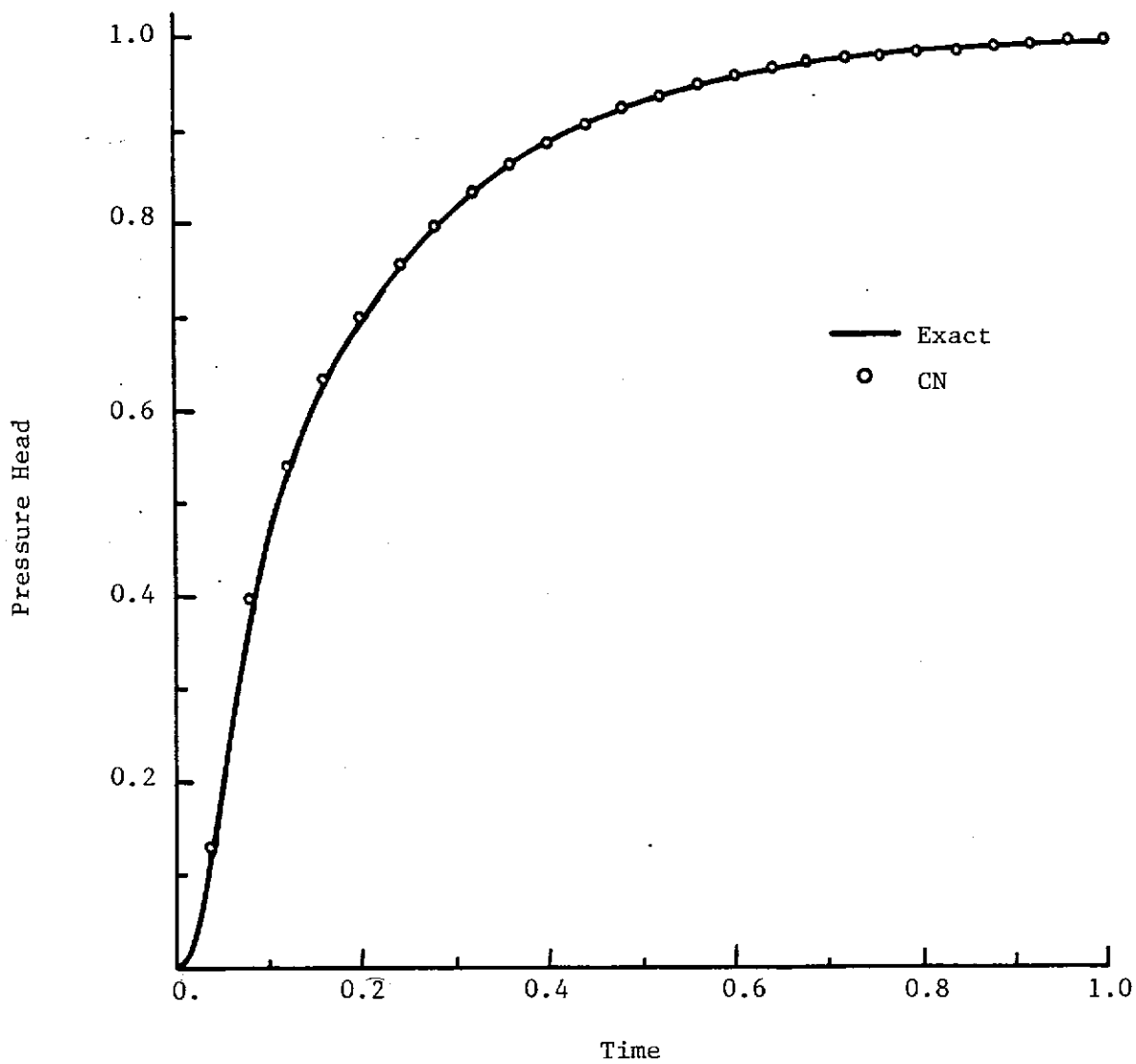HISTORIES AT NODE 25

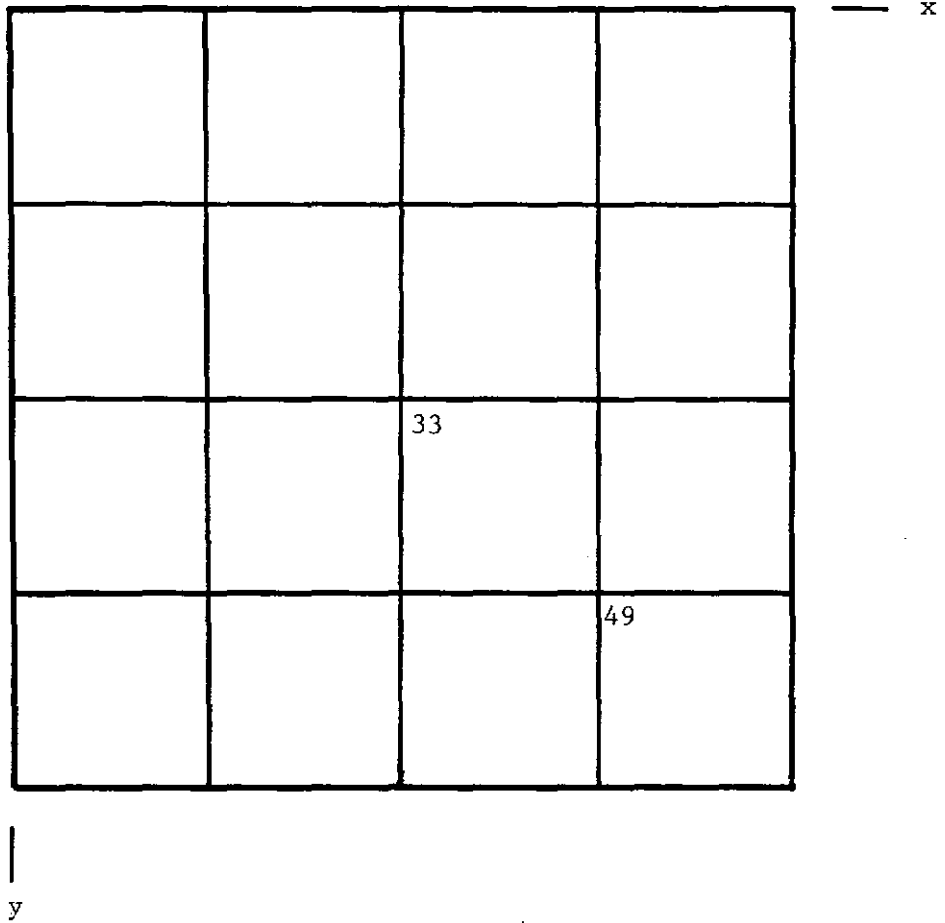FIG. IV.4 — ISOTROPIC AQUIFER PRESSURE HEAD
HISTORY AT NODE 14

51

FIG. IV.5 – FINITE ELEMENT MESH FOR THE
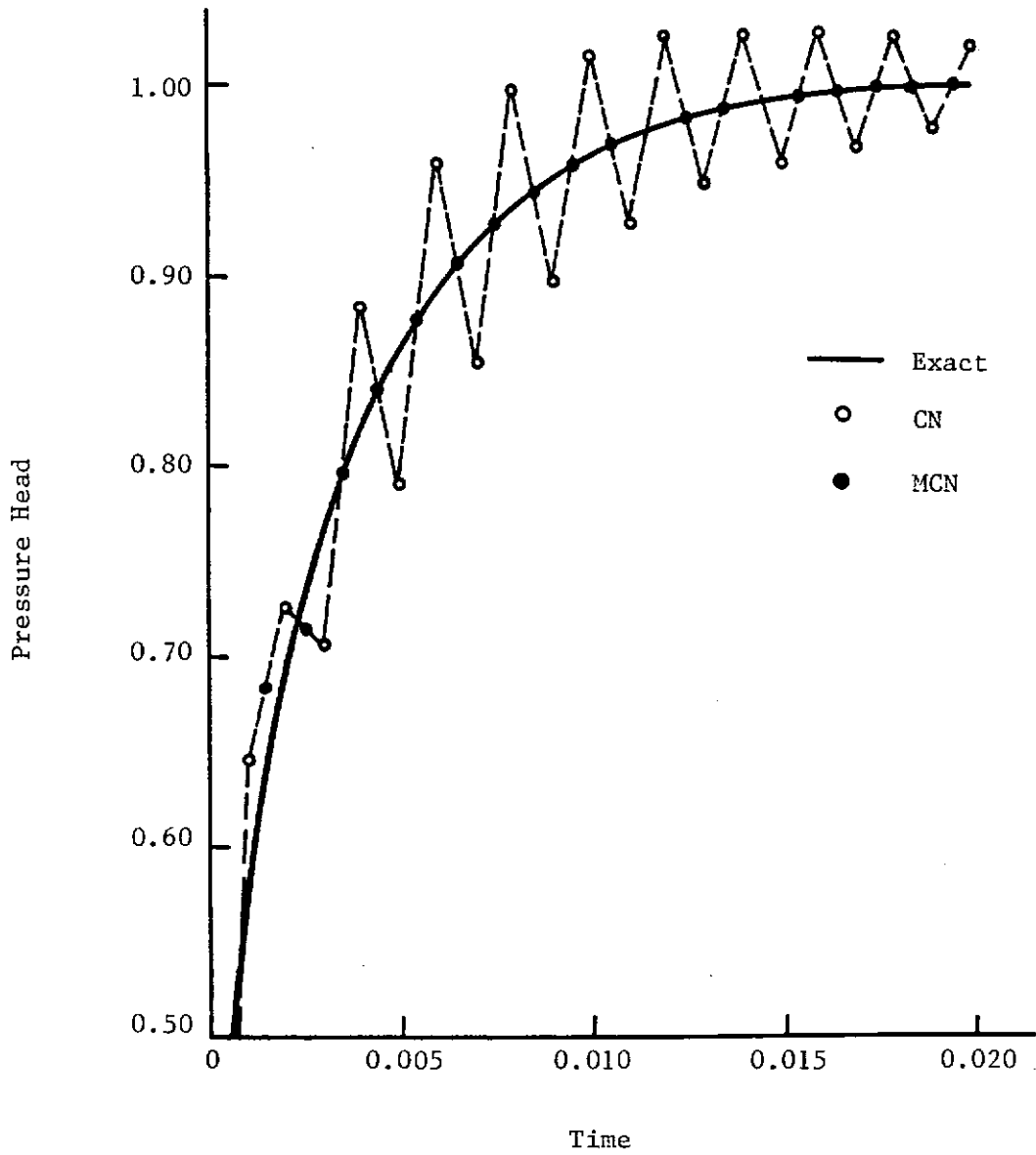ORTHOTROPIC AQUIFER ANALYSIS

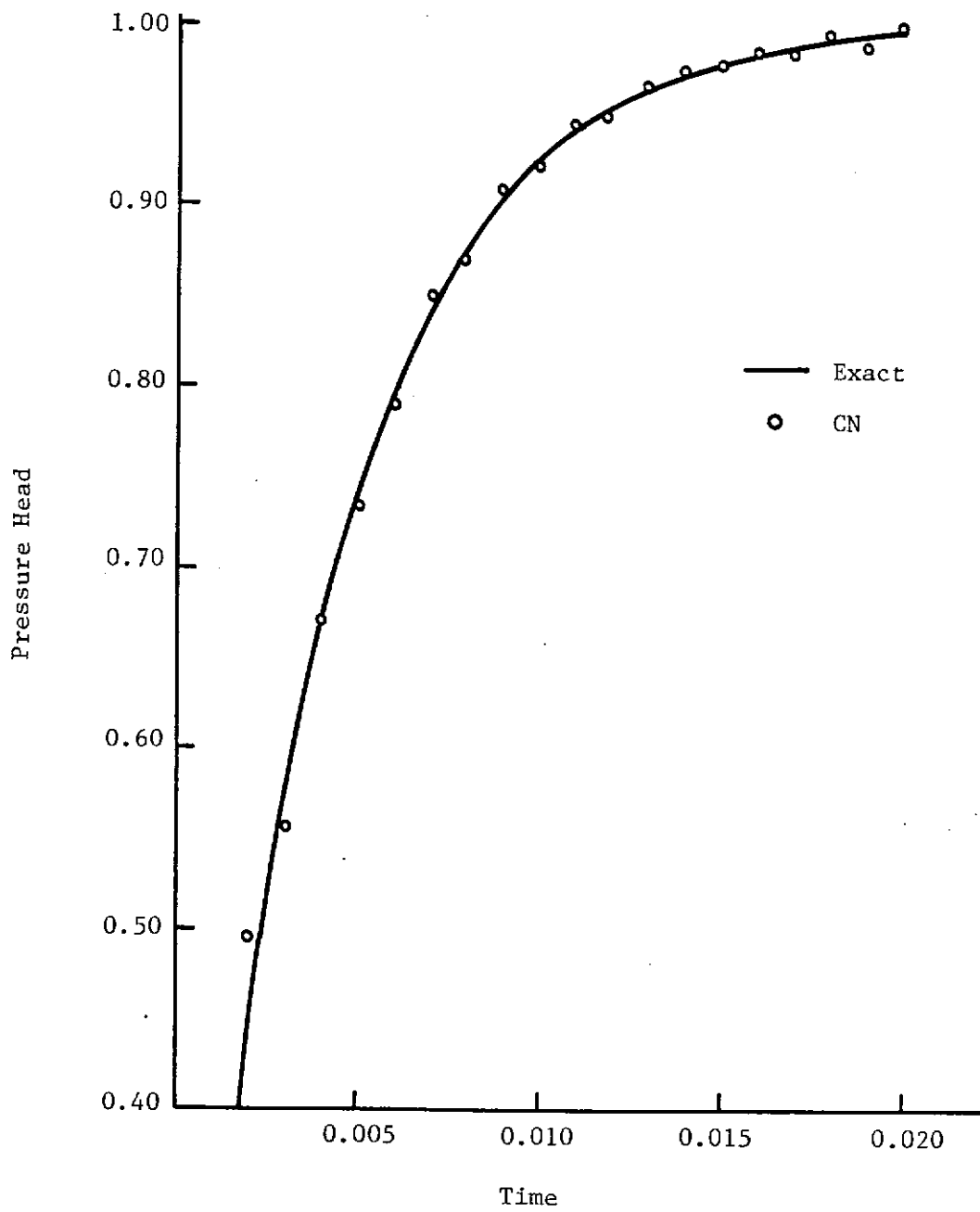FIG. IV.6 – ORTHOTROPIC AQUIFER PRESSURE
HEAD HISTORIES AT NODE 49

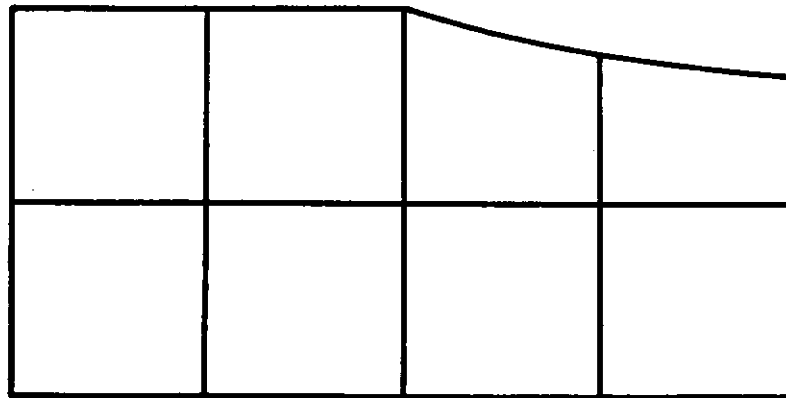FIG. IV.7 - ORTHOTROPIC AQUIFER PRESSURE HEAD HISTORY
AT NODE 33

(a) Moisture Content Contours

(b) Finite Element Mesh
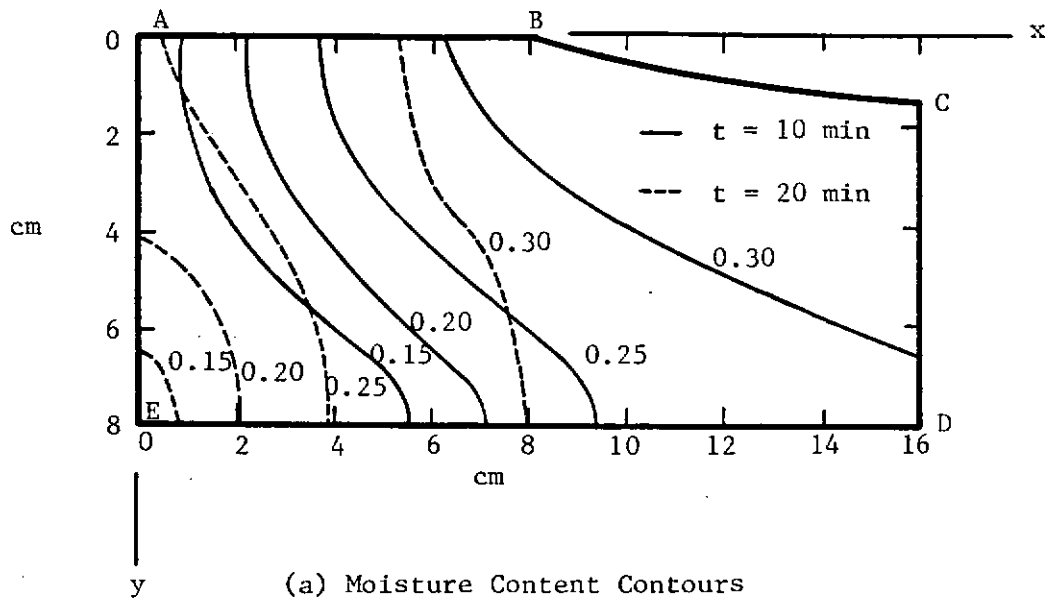
FIG. IV.8 - SOIL SLAB INFILTRATION PROBLEM

CHAPTER V

SUMMARY AND CONCLUSIONS AND FUTURE RESEARCH

V.1 SUMMARY AND CONCLUSIONS

The presented research was formulated to provide a scientifically based procedure for the analysis of subsurface flow in saturated-unsaturated porous media. The research enables a prediction of subsurface flow which can be coupled to other programs to predict contaminant migration, floods, resevoir capacity, moisture profiles, etc. In particular, groundwater contamination from environmental, domestic, industrial and agricultural sources has far reaching consequences in the safe utilization of groundwater supplies by domestic and industrial users.

The Galerkin finite element method is well suited for the solution of problems involving transient saturated-unsaturated flow in porous media. The finite element method coupled with the cubic spline representation of the material properties appears to be computationally efficient in overcoming difficulties arising from the nonlinear nature of such problems. Owing to its numerical efficiency as well as to its versatility, the finite element method offers several advantages over conventional finite difference techniques in dealing with saturated-unsaturated soils. In particular, the use of quadratic finite elements allows for greater spacial accuracy thus requiring much fewer elements and unknown pressure heads or moisture contents. The use of the modified Crank-Nicolson scheme was shown to result in far superior results than the Crank-Nicolson scheme for oscillatory prone simulations.

V.2 FUTURE RESEARCH

The developments of this research investigation has left this investigator with a wish list of investigative ideas. At the top of the investigation wish list would be the implementation and testing of the nonlinear seepage and infiltration/evaporation boundary conditions discussed in Chapter III. Obviously, this capability would enhance the computer model for simulating a wider variety of problems encountered by soil scientists and engineers. Once this is completed, a second item would be to utilize the model for simulating a layered unsaturated porous medium. The comparison of model results with field observations would strengthen the validity of the developed model. This wish may be possible in the near future as the result of research being conducted in the Department of Agricultural Engineering at the University of Kentucky (Warner et al., 1984).

Other investigative ideas include: implementing an automatic time increment scheme compatible with the single-step algorithm of this report, and modelling two-dimensional soil deformation. The automatic time increment strategy would initially utilize small time increments when the transient behavior is dominant. Whereas when the transient response is less dominant, larger time increments would be used. This obviously would improve simulation accuracy and efficiency.

The inclusion of two-dimensional soil deformation would permit realistic modelling of the soil consolidation and porosity. Further, many of the nonlinear material coefficient variations in subsurface flow are known or formulated in terms of the effective stress (e.g., Narasimhan, 1975; Narasimhan and Whiterspoon, 1977). Thus, a coupled soil deformation-flow model would allow for the calculation of effective stresses which would then be used to more realistically model the flow properties, possibly including

hysteresis behavior.

Finally, coupling the subsurface flow model to a contaminant transport model would allow for the simulation of contaminant migration. This coupling would have to include simulating contaminant transport in an engineered toxic waste site. The computer simulation comparison with field observations would result in an engineering design aide for disposing hazardous wastes.

REFERENCES

Bathe, K.J. and Wilson, E.L. (1976), Numerical Methods in Finite Element Analysis, Prentice-Hall, Chapter 8.

Bear, J. (1979), Hydraulics of Groundwater, McGraw-Hill, Chapters 4-6.

Blandford, G.E. and Tauchert, T.R. (1984), "Thermoelastic Analysis of Layered Structures with Imperfect Layer Contact," Computers and Structures, in press.

Bruch, J.C. and Zyvoloski, G. (1974), "Transient Two-Dimensional Heat Conduction Problems Solved by the Finite Element Method, " Int. J. Num. Meth. Engrg., Vol. 8, pp. 481-494.

Bruch, J.C. (1976), "Two-Dimensional Unsteady Water Flow in Unsaturated Porous Media," Finite Elements in Water Resources, W.F. Gray, G.F. Pinder and C.A. Brebbia, Editors, Pentech Press, pp. 3.3-3.19.

Campbell, G.S., (1974), "A Simple Method for Determining Unsaturated Conductivity from Moisture Retention Data," Soil Sci., Vol. 117, pp. 311-314.

Clapp, R.B. and Hornberger, G.M., (1978), "Empirical Equations for Some Hydraulic Properties," Water Resources Research, Vol. 14, pp. 601-604.

Cooper, H. (1966), "The Equation of Ground-Water Flow in Fixed and Deforming Coordinates," J. Geophys. Res., Vol. 71, pp. 4738-4790.

Cowper, G.R. (1973), "Gaussian Quadrature Formulas for Triangles," Int. J. Num. Meth. Engrg., Vol. 7, pp.405-408.

Feedes, R.A., Neuman, S.P. and Bresler, E., (1975), "Finite Element Analysis of Two-Dimensional Flow in Soils Considering Water Uptake by Roots: II Field Applications", Soil Sci. Am. Proc., Vol. 39, pp. 231-237.

Freeze, R.A., (1971), "Influence of the Unsaturated Flow Domain on Seepage Through Earth Dams," Water Resources Research, Vol. 7, pp. 929-941.

Freeze, R.A., (1972 a), "Role of Subsurface Flow in Generating Surface Run-off-Base Flow Contributions to Channel Flow," Water Resources Research, Vol. 8, pp. 609-623.

Freeze, R.A., (1972 b), A Physics-based Approach to Hydrologic Response Modeling Phase I: Model Development, Department of the Interior, OWRR No. 14-31-001-3694.

Gardner, W.R., Hillel, D. and Benyamini, Y. (1970), "Post Irrigation Movement of Soil Water to Plant Roots. I. Redistribution," Water Resources Research, Vol. 6, pp. 851-861.

Heubner, K.H. (1975), The Finite Element Method for Engineers, John Wiley and Sons, Chapter 2.

Hinton, E. and Campbell, J.S. (1974), "Local and Global Smoothing of Discontinuous Finite Element Functions Using a Least Squares Method," *Int. J. Num. Meth. Engrg.*, Vol. 8, pp. 461-480.

Hughes, T.J.R. (1977), "Unconditionally Stable Algorithms for Nonlinear Heat Conduction," *Comp. Meths. Appl. Mech. Engrg.*, Vol. 10, pp. 135-139.

IMSL Library Reference Manual (1982)

Moore, I.D. (1981), "Effect of Surface Sealing on Infiltration," *ASAE*, pp. 1546-1561.

Narasimhan, T.N. (1975), *A Unified Numerical Model for Saturated-Unsaturated Groundwater Flow*, Ph.D. dissertation, University of California - Berkeley, Berkeley, CA.

Narasimhan, T.N., Neuman, S.P. and Edwards, A.L. (1977), "Mixed Explicit - Implicit Iterative Finite Element Scheme for Diffusion - Type Problems: II. Solution Strategy and Examples," *Int. J. Num. Meth. Engrg.*, Vol.11, pp. 325-344.

Narasimhan, T.N. and Whiterspoon, P.A. (1977), "Unified Numerical Model for Saturated-Unsaturated Flow in Deformable Porous Media, Part I. Theory," *Water Resources Research*, Vol. 13, pp. 657-664.

Newman, S.P. (1973), "Saturated - Unsaturated Seepage by Finite Elements," *J. Hydl. Div.*, ASCE, Vol. 99, pp. 2233-2250.

Neuman, S.P. (1975), "Galerkin Approach to Saturated-Unsaturated Flow in Porous Media," *Finite Elements in Fluids - Viscous Flow and Hydrodynamics*, Vol. 1, R.H. Gallagher, J.T. Oden, C. Taylor and O.C. Zienkiewicz, Editors, John Wiley and Sons, Chapter 10.

Neuman, S.P., Feedes, R.A. and Bresler, E. (1975), "Finite Element Analysis of Two-Dimensional Flow in Soils Considering Water Uptake by Roots: I. Theory," *Soil. Sci. Soc. Am. Proc.*, Vol. 39, pp. 224-230.

Reeves, M. and Duguid, J.O. (1975), *Water Movement Through Saturated-Unsaturated Porous Media: A Finite Element Galerkin Model*, Oak Ridge National Laboratory, Oak Ridge, TN, ORNL-4927.

Rose, C.W. (1966), *Agricultural Physics*, Pergamon Press, Oxford.

Rubin, J. (1968), "Theoretical Analysis of Two-Dimensional Transient Flow of Water in Unsaturated and Partly Unsaturated Soils," *Soil Sci. Soc. Am. Proc.*, Vol. 32, pp. 607-615.

Tauchert, T.R. (1977), "A Residual Method with Lagrange Multipliers for Transient Heat Conduction Problems," *J. Heat Transfer*, Vol. 99, pp. 495-496.

Taylor, R.L. (1977), in O.C. Zienkiewicz, *The Finite Element Method*, Third Edition, McGraw-Hill, Chapter 24.

Terzaghi, K. (1925), "Settlement and Consolidation of Clay," *Engineering News*

<u>Record</u>, Vol. 26.

Warner, R.C., Barfield, B.J. and Sterling, H.J. (1982), <u>Demonstration and Evaluation of the Hydrologic Effectiveness of a Three Layer Surface Cover Under Stable and Subsidence Conditions</u>, Funded by: Environmental Protection Agency, Cincinnatti, OH, August.

Wood, W.L. and Lewis, R.W. (1975), "A Comparison of Time Marching Schemes for the Transient Heat Conduction Equation," <u>Int. J. Num. Meth. Engrg.</u>, Vol. 9, pp. 679-689.

Zienkiewicz, O.C. (1977), <u>The Finite Element Method</u>, Third Edition, McGraw-Hill, Chapters 7 and 8.